The Stratification Maxima of the Seasonally Varying Surface Layer in the Arctic Ocean's Beaufort Gyre

by

Peter Albert Roemer

B.S., United States Naval Academy (2013)

Submitted to the Department of Earth, Atmospheric and Planetary Sciences
in partial fulfillment of the requirements for the degree of

Master of Science

at the

MASSACHUSETTS INSTITUTE OF TECHNOLOGY

and the

WOODS HOLE OCEANOGRAPHIC INSTITUTION

September 2021

Author .....
Department of Earth, Atmosphere, and Planetary Sciences
Massachusetts Institute of Technology
August 31, 2021

Certified by .....
Sylvia Cole
Associate Scientist
Woods Hole Oceanographic Institution
Thesis Supervisor

Accepted by .....
Glenn Flierl
Chairman, Joint Committee for Physical Oceanography
Massachusetts Institute of Technology
Woods Hole Oceanographic Institution

The Stratification Maxima of the Seasonally Varying Surface Layer in the Arctic Ocean's Beaufort Gyre

by

Peter Albert Roemer

Submitted to the Department of Earth, Atmosphere, and Planetary Sciences
Massachusetts Institute of Technology
on August 31, 2021, in partial fulfillment of the
requirements for the degree of
Master of Science

Abstract

The Beaufort Gyre region of the Arctic Ocean is strongly stratified at the base of the wintertime mixed layer, which impedes the vertical transport of heat, energy, and other tracers. Ice-Tethered Profiler observations during 2004-2018 were used to characterize and investigate the seasonal and interannual variability of the strength, depth, density, and thickness of this highly stratified layer at the base of the mixed layer. This includes investigating the remnant stratification maximum, which formed when the summer mixed layer shoaled. Seasonally, the stratification maximum was never in a steady state. It was largest in October ($4.8 \times 10^{-3} rad^2/sec^2$) and decreased during all winter months (to $2.3 \times 10^{-3} rad^2/sec^2$ in June), indicating that surface forcing and interior vertical mixing were never in equilibrium during the year. Interannually, the period from 2011-2018 had a higher stratification maximum than then the period from 2005-2010 regardless of the season. The remnant stratification maximum was consistently weaker than the winter stratification maximum from which it formed. The initial evolution of the remnant stratification maximum is used to estimate an effective vertical diffusivity of order $10^{-6} m^2/s$. No significant geographic variability was found, in part due to high temporal and small scale variability of the stratification maximum layer. Implications for heat transport through to the sea ice cover are discussed.

Thesis Supervisor: Sylvia Cole
Title: Associate Scientist
Woods Hole Oceanographic Institution

Acknowledgments

It would be impossible to recognize everyone who contributed to the successful completion of this this, but I will attempt it. The completion of this thesis was the result of an incredible amount of hard work and mentoring from my adviser, Dr. Sylvia Cole. Words fail to due to justice to the amount of effort she put into my development, and I will be forever grateful for that. It would have been impossible to get a better teacher and mentor. Joint Program staff, especially Kris Kipp and Leanora Fraser were invaluable for the transition to MIT, and the unprecedented COVID times. The faculty at WHOI were excellent teachers and scientists who welcomed Navy students with open arms, making my two years at Woods Hole incredibly valuable. The Navy provided funding for my education, and allowed me to take time out of my career to pursue academics. Finally, the neverending support of my patient family and friends got me to the finish line. Without all of the above, none of this would have happened.

Contents

List of Figures

List of Tables

Chapter 1

Introduction

Arctic sea ice plays a large role in the global climate system, and has undergone significant changes in the past several decades. The Arctic is one of the major reservoirs of ice in the global climate, and the continued evolution of the ice pack is relevant to several stakeholders. First, the ice contributes to the albedo of the planet, and significant gain or loss of ice could lead to changes in the global climate due to changes in the amount of solar energy reflected from the earth (Curry et al., 1995). Second, the loss of sea ice is hypothesized to have an oversized impact on the Atlantic meridional overturning circulation, a key source of transport in the global current system (Sévellec et al., 2017). We can also see the impact on the biological productivity of the region, and as the sea ice extent decreases and the open water regions become more extensive seasonally and interannually, it will become more and more relevant to international shipping (Frey et al., 2020) (Farré et al., 2014). Sea ice extent has already changed in the past several decades, with the annual mean sea ice index (total area with sea ice concentration above 15 percent) decreasing over 17 percent, or nearly 2 million square kilometers since 1980, and reaching a recorded minimum in 2012 (Kwok, 2018).

Geographically, the Arctic is divided into several basins, the largest of which are the Canada basin north of Canada, and the Eurasian basin, north of Russia. There are only two significant flow paths from the world ocean to the Arctic: through the Bearing Strait and the Fram Strait, which places the Arctic Ocean in a state of relative isolation. Because of this isolation, local processes play a large role in shaping how the region behaves. Within the Canada Basin is the Beaufort Gyre, which is a large anti-cyclonic current system that

occupies the central part of the basin. The Beaufort Gyre acts as the largest reservoir of fresh water in the region, since the gyre sees both a large amount of sea ice melt and a large amount of river runoff. This freshwater is driven into the center of the Canadian Basin by the Ekman convergence generated by the dominant regional wind patterns, and the subsequent downwelling creates a lens of freshwater that sits on top of a saltier ocean interior.

In this paper, we examine Ice-Tethered Profiler (ITP) records in the Beaufort Gyre in all seasons, and specifically those records that cover a transition between the winter and summer seasons in order to characterize and investigate the thin stratification maximum layer that resides beneath the mixed layer base. As described in the remainder of this introduction, this is an important and underobserved region of the ocean that is also difficult to model numerically.

1.1 Watermasses and significance

In the vertical, three major water masses comprise the Arctic Ocean: a top layer of fresh, cold water in the upper 10s of meters, Atlantic Water or Pacific and Atlantic water underneath, which is warmer and saltier than the surface waters, and Arctic Bottom Water in the lowest depths, which is both cold and salty. Atlantic water and Pacific summer water arise from the relatively salty waters in the upper latitudes of the Atlantic and Pacific subducting as they enter the Arctic ocean. Because of their high salinity relative to the surface waters in the Beaufort Gyre, these salty water masses end up being more dense than the surface water, despite being warmer. This temperature profile that is not monotonically decreasing with depth is characteristic of the Beaufort Gyre. The large quantity of surface freshwater sets up a steep halocline that separates a relatively large amount of heat carried in the Pacific Summer Water from the mixed layer and ice cover .

Water above the halocline exhibits significant seasonal variability. The most significant seasonal changes are in the upper fifty meters of the water column with water becoming warmer, fresher, and lighter as winter changes to summer, and colder, saltier, and denser as summer changes into winter. These changes are largely driven by ice formation and melt. In the winter, the brine rejection associated with ice formation creates salty water near the surface. The brine is much saltier than the seawater around it, and the brine near the surface sinks causing convective mixing which deepens the mixed layer. This process occurs over

several months, with the mixed layer deepening between three and five meters per month during the winter. As the ice melts, it turns into freshwater, which is roughly the same temperature as the near surface waters, but it significantly less salty (and because of this, approximately one degree warmer) . Unlike brine, this freshwater is inclined to stay near the surface, and while some diffusion and mixing does occur, overall, this shifts the mixed layer shallower. This transition from a characteristic winter profile to a characteristic summer profile happens abruptly. In contrast to the winter, the shoaling of the mixed layer can happen on the order of meters per day. This occurs because the freshwater remains on the surface, significantly altering the surface density, instead of sinking and entraining lighter water the way the brine does. In both the summer and the winter, the strong stratification of the mixed layer base plays a large role in isolating the mixed layer and sea ice from the heat carried in the Pacific Summer Water (Shimada et al., 2006).

1.2 Stratification and significance

Tracers in the ocean (e.g., salt, heat, or nutrients) more easily spread along density surfaces, as opposed to across them (McDougall, 1984). Vertical variations in density thus play a large role in shaping the movement of these tracers. Stratification near the surface contributes significantly to the interactions between the ocean and the atmosphere, and in the case of the Arctic Ocean, between the ocean and the sea ice. Globally, upper ocean stratification in particular has been strengthening over the past 60 years, with important implications for biological productivity and deep water formation (Yamaguchi and Suga, 2019). Climatology shows that upper latitudes, including the Arctic Ocean tend to have generally higher stratification to begin with, due in large part to freshwater fluxes (Li et al., 2020).

The most strongly stratified water resides in the uppermost meters of the halocline just beneath the seasonally variable mixed layer. This layer of strong stratification is roughly 4-5 meters thick, but plays a very important role in separating the heat in the lower waters from the surface. It is the barrier between the surface and interior processes, and one feature of the transition layer that is affected by both the surface and interior processes. Changes in stratification could impact how easily heat diffuses across the layer, and changes in depth could impact how easily a synoptic scale weather event (eg a large storm) could disrupt the stratification, potentially making it much easier for lower depth heat to reach the surface.

The stratification at the base of the mixed layer can play a large role in the evolution of the surface ice cover in the Beaufort Gyre. Relatively warm and salty Pacific Summer Water lies beneath the mixed layer, but the heat there is isolated from the upper waters because of the stratification at the mixed layer base. This separation of the heat from the surface plays a large role in regulating the sea ice growth: the separation of the heat prevents ice from being melted if the heat was entrained in the mixed layer.

Despite the importance of stratification at the base of the mixed layer, it is historically not a simple feature to quantify. Due to limited ship observations in winter, and subsurface moorings that do not observe the upper tens of meters of the water column, the ITP record fills a gap in high resolution measurements of the ice covered regions of the ocean. While it tends to be studied outside the Arctic (Thomson and Fine, 2003; Brainerd and Gregg, 1993; Yamaguchi and Suga, 2019; Johnston and Rudnick, 2009; Dohan and Davis, 2011), studies of the stratification maximum inside the Arctic Ocean are less prevalent.

1.3 Trends and Climatology

The reservoir of freshwater in the Beaufort Gyre, and thus its strong stratification, is maintained in part by the circulation of the sea ice and upper ocean. Momentum transfer to the ocean occurs when there exists a difference in velocity between the wind and sea surface (or between the sea surface and the ice on top). This resultant stress causes Ekman pumping and consequently changes in the distribution of freshwater in the Beaufort Gyre. However, because the ice and ocean move at different speeds, stress calculations based on wind alone fail to provide the full picture of Ekman transport in the Beaufort Gyre. The physical motion of the ice generates turbulence, which causes mixing, and consequently, deepening of the mixed layer. This mixing is dependent on numerous factors, including wind speed, ice roughness, ice draft, and total ice concentration, and the relative speed between the ice and the ocean. In fact, numerical and observational studies show that increased ice cover acts as a governor on the stress in the upper ocean (Dewey et al., 2018) (Meneghello et al., 2018). This happens when the ocean current exceeds the speed of the surface ice, reversing the sign of the Ekman transport, and thus limiting the convergence of freshwater and consequently the depth and strength of the halocline. A strengthened halocline means that there exists more freshwater near the surface and the ocean heat content is more insulated from the ice

cover.

Two significant trends emerge in the climatology of the Beaufort Gyre in the past twenty years or so. The first is that the Beaufort Gyre has undergone relatively significant freshening, which is dominated by the change in Ekman transport, which is related to the sea ice conditions as described above (Proshutinsky et al., 2019). The freshening was most significant over the 2003-2008 period, after which is stabilized until 2013, after which it increased through 2016. This freshening happens at the same time we examine the mixed and remnant layer dynamics.

The second major dynamical change is that of sea ice in the Beaufort Gyre. In the Arctic as a whole, sea ice coverage has been declining on a decadal time scale. There is annual variability, with local minima in 2007, 2012, and 2016. In addition to the mixing effects discussed before, reduced ice cover allows additional solar heating of the ocean. Again, this timeframe overlaps with the period of time where we examine mixed layer and remnant layer dynamics.

Chapter 2

Data

2.1 Ice-Tethered Profilers

We consider temperature and salinity observations from Ice-Tethered Profilers (ITPs) (Toole et al., 2011). An ITP is moored to the surface of an ice floe and has a profiler that travels up and down a weighted wire several times a day to sample conductivity, temperature, and pressure (Toole et al., 2011). Profiles are nominally from 5 meters to 750 meters depth. The data is then quality controlled, processed, and binned into 1 meter increments (Krishfield et al., 2008a). For the majority of the records, sampling occurred twice a day, separated by 6 and 18 hour increments. Some records sampled 4, 6, or 8 times a day at uniform intervals. The entire ITP record began in 2004 and we include data through 2018 in this study.

We consider profiles in the Beaufort Gyre region of the Arctic ocean which we define as bounded by the latitude line south of 80 degrees North, the longitude lines west of 120 degrees West and the line east of 180 degrees East. This provides 44 ITP records with 32553 profiles. The number of ITPs in the Beaufort Gyre varies in time (Fig 2-1). Observation from multiple ITPs simultaneously did not begin until 2006, and there is a significant period of time in 2016 when no ITP coverage existed. Table (2.1) provides the temporal and geographic boundaries of each ITP record included in this study.

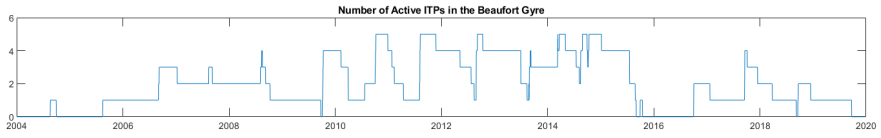

Figure 2-1: The monthly number of Ice-Tethered Profilers in the Beaufort Gyre Region between 2004 and 2020

We additionally consider a subset of ITP records by examining only those ITPs that begin in March through May (or earlier), and then continue through August (or later). This results in 19 records, of which 16 were sufficient for analysis. Such records are in bold in Table (2.1) and span the 2005-2018 time period.

2.2 Ice Concentration

Ice concentration was obtained from the National Snow and Ice Data Center (NSIDC) AMSR-E/Aqua L3 Daily values. This product provides a gridded daily value of sea ice concentration in the polar regions. The data is gridded to a polar stereographic projection with horizontal resolution of 12.5km by 12.5km at 70 degrees N. For each ITP profile the ice concentration associated with the closest grid value in the NSIDC data set was used. Thus, over the course of a calendar day, any changes in a particular record's ice concentration are due to spatial variations, but day to day changes are due to both temporal and spatial changes in ice concentration. There is uncertainty in ice concentration measurements, including errors for thin ice, and that the gridded ice concentration is matched with the ITP location for that time.

2.3 Ice Draft

Ice draft is considered from four moorings in the Beaufort Gyre collected as part of the WHOI Beaufort Gyre Exploration Project (Krishfield et al., 2014). Each of four moorings includes an upward looking sonar (ULS) to observe the ice draft. The number and locations of active moorings varied from year to year (Figure 2-2). Each ULS sends a pulse upwards approximately once every three seconds to determine the depth of the ice above it. Here, we consider the median of ice draft values in each calendar day and consider seasonal and interannual variations to be representative of the gyre's ice draft. This provides a time series of daily median ice drafts from August of 2003 through September of 2018 that characterizes the seasonality and interannual variability of ice thickness (Figure 2-3).

ITP	Start Date	End Date	Total Profiles	Daily Profiles	Min Lat	Max Lat	Min Lon	Max Lon
1	**08/16/05**	**01/08/07**	**2043**	**4**	**74.32°**	**79.2°9**	**-150.13°**	**-130.35°**
2	08/20/04	09/29/04	244	6	76.57°	77.17°	-141.38°	-134.12°
4	**09/03/06**	**08/17/07**	**698**	**2**	**78.12°**	**79.5°**	**-153.06°**	**-139.24°**
5	**09/08/06**	**09/07/07**	**1095**	**3**	**75.52°**	**76.69°**	**-148.89°**	**-137.92°**
13	**08/14/07**	**09/08/08**	**876**	**2**	**72.91°**	**79.98°**	**-150.23°**	**-130.15°**
18	**08/17/07**	**10/09/08**	**914**	**2**	**73.98°**	**79.15°**	**-146.1°**	**-131.71°**
21	**08/04/08**	**09/23/09**	**832**	**2**	**72.55°**	**79.99°**	**-150.01°**	**-134.51°**
32	10/04/09	02/09/10	257	2	79.55°	80°	-151.52°	-138.65°
33	**10/07/09**	**01/25/11**	**952**	**2**	**74.61°**	**78.12°**	**-159.89°**	**-138.37°**
34	10/11/09	03/30/10	342	2	73.22°	74.78°	-161.07°	-134.13°
35	10/09/09	03/31/10	1357	8	74.57°	77.36°	-143.86°	-134.77
39	07/23/10	12/28/10	317	2	42.94°	42.95°	-122.09°	-122.08°
41	**10/03/10**	**10/11/12**	**1480**	**2**	**73.84°**	**79.19°**	**-154.24°**	**-131.95°**
42	10/05/10	04/15/11	386	2	75.96°	77.66°	-151.36°	-143.52°
43	10/08/10	02/11/11	253	2	74.39°	76.73°	-145.51°	-135.16°
52	08/06/11	11/23/11	378	4	77.8°	79.39°	-141.31°	-132.24°
53	**08/05/11**	**08/13/12**	**750**	**2**	**73.57°**	**77.66°**	**-159.71°**	**-137.51°**
54	08/07/11	07/23/12	1055	2	72.65°	77.29°	-168.13°	-136.86°
55	08/08/11	05/08/12	547	2	71.49°	76.1°	-176.44°	-136.93°
62	**09/05/12**	**08/12/13**	**686**	**4**	**72.25°**	**77.65°**	**-159.05°**	**-134.67°**
64	**08/29/12**	**08/24/13**	**1123**	**4**	**72.83°**	**79.33°**	**-160.26°**	**-134.66°**
65	08/28/12	06/29/13	903	4	74.58°	79.99°	-149.86°	-137.17°
66	08/28/12	06/29/13	903	4	74.58°	79.99°	-149.86°	-137.17°
68	08/28/13	05/03/14	682	4	74.68°	76.76°	-163.09°	-139.63°
69	08/29/13	03/12/14	477	4	74.62°	75.68°	-167.72°	-140.16°
70	08/25/13	07/15/14	2585	8	74.37°	77.24°	-156.51°	-138.6°
77	**03/10/14**	**10/02/14**	**1659**	**8**	**73.3°**	**76.01°**	**-158.96°**	**-134.99°**
78	**03/11/14**	**08/06/14**	**1180**	**8**	**73.77°**	**74.7°**	**-146.95°**	**-135.13°**
79	**03/21/14**	**09/29/14**	**1195**	**8**	**74.06°**	**75.53°**	**-147.87°**	**-134.88°**
81	08/17/14	07/18/15	671	2	77.54°	79.99°	-159°	-133.72°
84	10/13/14	01/06/15	172°	4	74.88°	75.98°	-150.33°	-139.86°
85	**10/08/14**	**09/02/15**	**660**	**4**	**74.52°**	**79.15°**	**-154.6°**	**-136.48°**
86	**08/16/14**	**08/26/15**	**754**	**4**	**75.28°**	**77.66°**	**-155.68°**	**-140.24°**
87	08/29/14	07/18/15	647	2	75.5°	80°	-154.43°	-132.69 °
88	09/30/15	10/15/15	31	2	77.58°	78.72°	-142.01°	-138.47°
97	**10/03/16**	**10/05/17**	**736**	**4**	**72.38°**	**79.14**	**-150.89**	**-133.53**
99	10/02/16	01/21/17	224	2	74.19°	77.88°	-144.98°	-132.82°
100	09/19/17	12/15/17	176°	2	78.09°	79.97°	-152.09°	-142.98°
101	09/17/17	03/26/18	382	2	76.97°	79.98°	-137.22°	-126.52°
107	**09/19/18**	**09/23/19**	**740**	**4**	**72.99°**	**79.7°8**	**-157.63°**	**-133.83°**
108	**09/18/17**	**09/08/18**	**1003**	**4**	**70.07°**	**79.97°**	**-145.61°**	**-122.41°**
109	09/22/18	12/15/18	169	2	74.75°	77.52°	-144.41°	-136.71°

Table 2.1: Statistics for each of the ITP records in the Beaufort Gyre Region

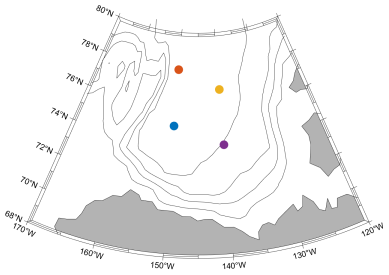

Figure 2-2: Locations of moorings that observed ice draft from the WHOI Beaufort Gyre Exploration Project. Blue: Mooring A (2004-2018) Red: Mooring B (2004-2018) Yellow: Mooring C(2004-2008) Purple: Mooring D(2006-2018)

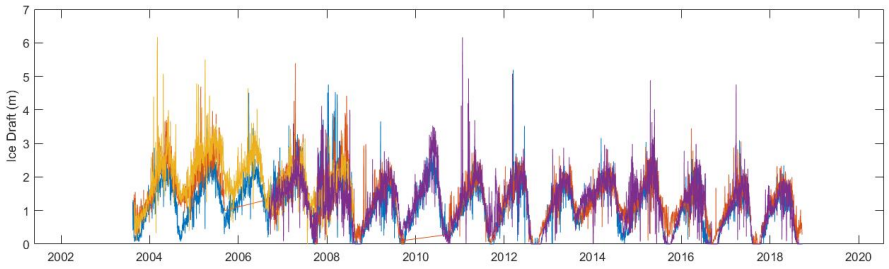

Figure 2-3: Median daily ice draft from the WHOI Beaufort Gyre Exploration Project. Blue: Mooring A (2004-2018) Red: Mooring B (2004-2018) Yellow: Mooring C(2004-2008) Purple: Mooring D(2006-2018)

2.4 Wind Speed

We use wind speed from the European Center for Medium Range Weather Forecasts (ECMWF) hourly reanalysis product. This provided 10m meridianal and longitudinal wind speeds at quarter degree resolution. The directional wind speeds were converted into a wind magnitude, and in a manner similar to that of the ice concentration, the closest grid point (in both time and space) to a given ITP profile was examined.

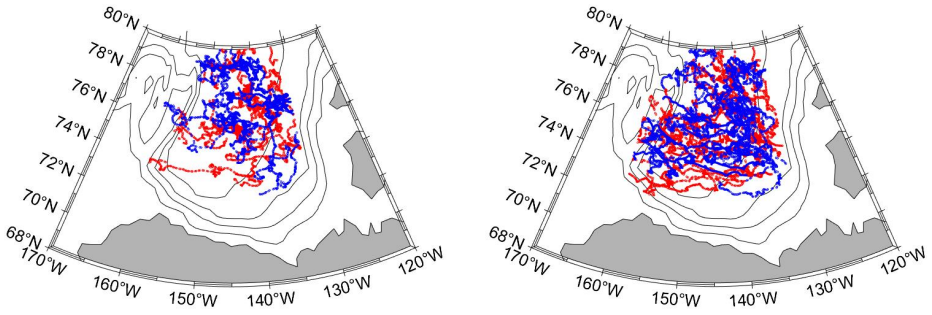

Figure 2-4: The geographic locations of all ITP profiles in the Beaufort Gyre considered in this study. Left panel shows 2005-2010. Right panel shows 2011-2018. Colors indicate profiles collected during Dec - May (blue) and Jun - Nov (red). Bottom depth contours are at 500, 1500, 2500, and 3500 meters.

Chapter 3

Methods

3.1 Temperature, Salinity, and Stratification

The processed ITP data includes the location and time of each profile, as well as the temperature, salinity, and pressure in 1 m depth bins. (Toole et al., 2011; Krishfield et al., 2008b) The Gibbs Seawater Toolbox was used to determine ice speed, absolute salinity, conservative temperature, and density at each depth for every profile. N^2 was calculated at each point in depth as:

$$N^2 = \frac{-g}{\rho}\frac{\partial \rho}{\partial z}$$

where g is the gravitational acceleration, ρ is the density and dz is the 1m vertical difference.

3.2 Mixed layer and stratification maximum layer

Mixed layer depth was determined for each profile and defined using a density threshold of 0.25 kg/m^3 from the shallowest observation, provided this observation was shallower than 20 meters depth. If such a shallow density did not exist, the mixed layer depth was not defined, and the profile was not considered. This could have occurred because a profiler did not travel the full length up the wire (eg due to strong ice speeds or large wire angles), or the profile was excessively short and the profiler did not travel far enough down the wire.

The maximum stratification, N^2_{max}, is the maximum value of stratification in each profile. The depth where this stratification occurs is the depth of stratification maximum $z_{N^2 max}$ and generally was at most a few meters deeper than the mixed layer base. The thickness of the

stratification maximum layer is taken to be its full-width at half-max (FWHM). The FWHM is defined as the distance between the depths above and below the stratification maxima where the stratification is half of the maximum value (e.g., Figure 3-1). Specifically, and to avoid interpolating in the vertical, the distance above and below the maximum is defined by the nearest depth where stratification is less than half the peak value.

3.3 Remnant mixed layer and remnant stratification maximum layer

To define the depth of the remnant stratification maximum, which approximates the depth of the remnant mixed layer, the following steps are taken (Figure 3-2):

1. A subsection of each profile was identified that was between 30 and 70 m depth and at least 10 m deeper than the mixed layer depth. These ranges were chosen to avoid identifying stratification maxima from the summer mixed layer, or other abnormalities, such as the tops of eddies.

2. The remnant layer stratification maximum, N^2_{RL}, was then defined as the maximum stratification value over this subsection of the profile. The remnant layer depth, z_{RL}, is the depth at which this maximum value occurs.

We use the term remnant mixed layer (after (Brainerd and Gregg, 1993)) to refer to the portion of the water column between the summer mixed layer base and the depth of the N^2_{max}. This definition was applied to all profiles, and could produce a remnant layer during any season. This occurred both when it was seasonally acceptable, but also at other times, such as when the ITP transited through a large eddy with subsurface stratification peaks. To analyze only relevant data, all remnant layer depths and remnant layer stratification values from before a defined transition time, $t_{transition}$ were ignored. This transition time is representative of when the formation of the summer mixed layer occurs (see section 3.6). There are 32553 total profiles, of which 26518 exhibit a mixed layer, and 4150 exhibit a remnant layer. In cases where a remnant mixed layer and a mixed layer both exist, the stratification may never decay to half of its maximum value. In this case, the FWHM was defined by the distance between the stratification maximum and the minimum value between

the two local maxima. This occurred in less than 1 percent of profiles. Table 3-1 summarizes the notation used for the mixed layer and remnant mixed layer.

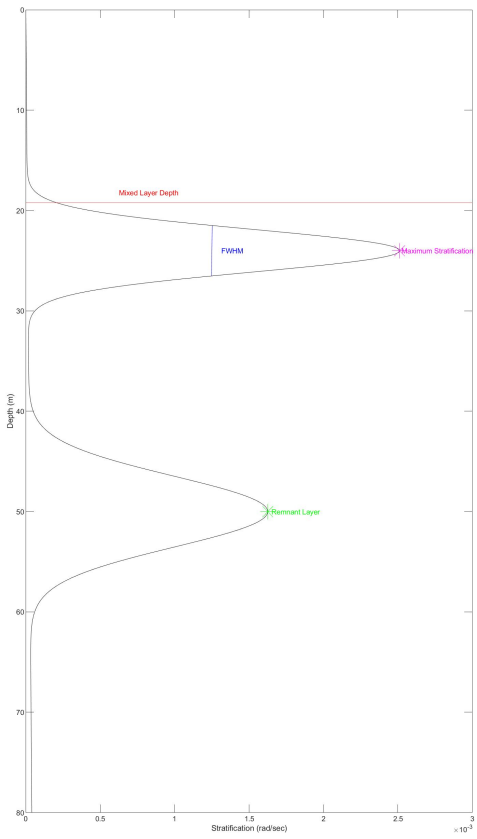

Figure 3-1: An idealized stratification profile (black line). Mixed layer depth is given by the red line. The FWHM (blue line), maximum stratification value (magenta star), and remnant layer depth (green star) are indicated.

3.4 Heat Content

Ocean heat content is considered, including within the stratification maximum layer and the Pacific Summer Water layer. The heat content of a given portion of the water column is defined as :

$$OHC = \int_{z_0}^{z_1} \rho_0 c_p (T(z) - T_{freezing}) dz \tag{3.1}$$

Name	Units	Description
z_{ML}	meters	Mixed Layer Depth
z_{RL}	meters	Remnant Layer Depth
z_{N2max}	meters	Maximum Stratification Depth
N^2_{max}	rad-sec^{-1}	Maximum Stratification Value per profile
N^2_{RL}	rad-sec^{-1}	Stratification value at the Remnant Layer
N^2_{ML}	rad-sec^{-1}	Stratification value at the Mixed Layer
OHC	Watts-meter^{-1}	Oceanic Heat Content per meter of depth
$FWHM$	meters	Full Width at Half Maximum
$t_{transition}$	date	Transition time between winter and summer

Table 3.1: List of Variables Used

Here, z_0 and z_1 are the bounds of the region being considered, ρ_0 is a nominal density (1020 kg/m^3), c_p is the specific heat capacity, $T(z)$ is the conservative temperature at a given depth, and $T_{freezing}$ is the freezing temperature given for water at equal pressure and salinity to the water who's temperature is being considered. Heat content is estimated for the mixed layer (surface to the mixed layer depth) and for the remnant layer (mixed layer depth to the remnant layer upper FWHM depth), as well as for maximum stratification layer (within its FWHM) and the PSW layer, which we take to be the 1025 kg/m^3 isopycnal (Timmermans et al., 2014).

3.5 Monthly Composite Statistics

We additionally considered ITP observations in a monthly sense. In a given calendar month, the median value of all profiles from all ITPs was considered. In the aggregation, a profile was weighted by sampling frequency such that a record that sampled at a rate that was half as fast as another record would be weighted twice. This ensured that the dominant value did not arise solely due to the number of profiles a record had on a monthly basis and each record was equally weighted.

3.6 Winter to Summer Transition

The significant shoaling of the mixed layer that occurred at the beginning of summer is used to define a transition time ($t_{transition}$), or the date at which the mixed layer shoaled. While not in exact alignment with meteorological summer, we use the term winter-summer transition to refer to the shoaling of the mixed layer as it separates winter conditions with a

deeper mixed layer from summer conditions with a shallow mixed layer and remnant mixed layer. The transition time was defined as the first day that meets the following three criteria:

- The mixed layer was 10 meters shallower than the average mixed layer depth in the March through May time period
- The mixed layer remained shallower than that average depth for 7 consecutive days.
- The transition time was after May 31st.

For all profiles that had a well defined winter mixed layer and a well defined remnant layer, this method matched with visual determinations of the transition time (e.g., Figure 3-2).

Of the available ITP data sets, 44 ITP records had data in the Beaufort Gyre, 28 cover the proper time period to determine a transition time, of which 12 show a transition occurring in sufficently high resolution to accurately determine a transition date and perform follow on analysis of the remnant stratification layer.

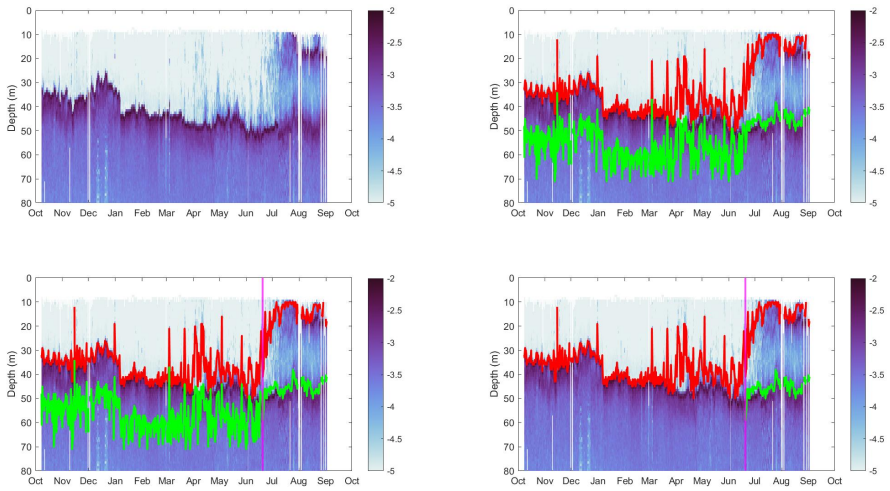

Figure 3-2: Timeseries of Log stratification profiles for ITP 85. Top Right: With mixed layer (red) and initial remnant layer (green) added. Bottom Left: With transition date (magenta line) added. Bottom Right: With remnant layer values prior to the transition time removed.

Chapter 4

Results

4.1 Seasonal Variability

The stratification maximum layer exhibited large seasonal variability which includes the development and erosion of the remnant mixed and stratification layers. Here, we examine the variability across seasons, contrasting wintertime and summertime conditions.

An example record, ITP-64, shows conditions typical of the Beaufort Gyre and its seasonal cycle. (Figure 4-1). During most months, the stratification maximum layer is clearly distinguishable from the halocline or remnant stratification maximum layer below by strong gradients in temperature, salinity, density, and stratification. The stratification maximum layer is less distinguishable during the formation of the summer stratification maximum layer and remnant stratification maximum layer in July. In the upper 50m, the seasonal cycle consists of warmer, fresher, and less dense waters in summer, and colder, saltier, denser waters in the winter. At 10 meters depth for ITP 64, salinity varied between 26 and 30 psu, and reached its maximum in February and minimum value in August. Temperature near the surface remained consistently between -1.5 and -1 , regardless of the time of year. This is characteristic of ice-covered waters where the stratification maximum layer is very near the (salinity dependent) freezing temperature. As density is most heavily dependent on salinity at these temperatures, seasonal variations in density in the upper portion of the water column were nearly identical to those of salinity. The stratification time series (Fig 4-1) shows that early in the year, the upper portion of the water column was well mixed, with a summer stratification maximum that formed in July and gradually mixed deeper throughout the fall. This stratification maximum in ITP 64 resided slightly deeper than the

stratification maximum layer base, which was characteristic of all ITPs. Overall, the stratification maximum seasonally ranged from 15m to 50m in depth, and from 2-3 rad^2/sec^2 to 4-5 rad^2/sec^2 in magnitude. The depth of the stratification maximum increased from summer through to the following spring.

The development of the remnant stratification maximum layer occured when the summer stratification maximum layer formed, alongside a remnant stratification maximum layer at approximately the depth of the previous winter's stratification maximum layer. The remnant stratification maximum layer remained visible from August to November at the approximate depth and density of the winter stratification maximum layer from which it formed. We refer to this region as the remnant stratification layer (analogous to the remnant stratification maximum layer residing at similar depths and densities to the winter stratification maximum layer from which it formed).

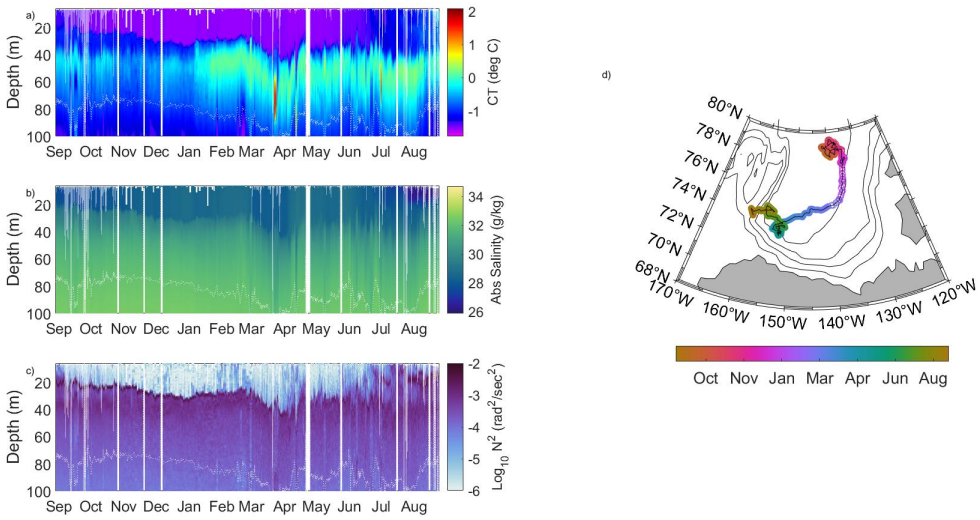

Figure 4-1: Timeseries of conservative temperature (top), absolute salinity (middle), and log stratification (bottom) for ITP 64, covering 2012-2013. Dashed white line indicates depth of the $1025 kg/m^3$ isopycnal. Right plot describes the location of the ITP.

4.1.1 Wintertime Conditions: December through May

We first consider the stratification maximum layer during December through May, when the stratification maximum layer is seasonally deep. During these months, ice concentration was typically near one hundred percent, the remnant layer from the previous year had largely

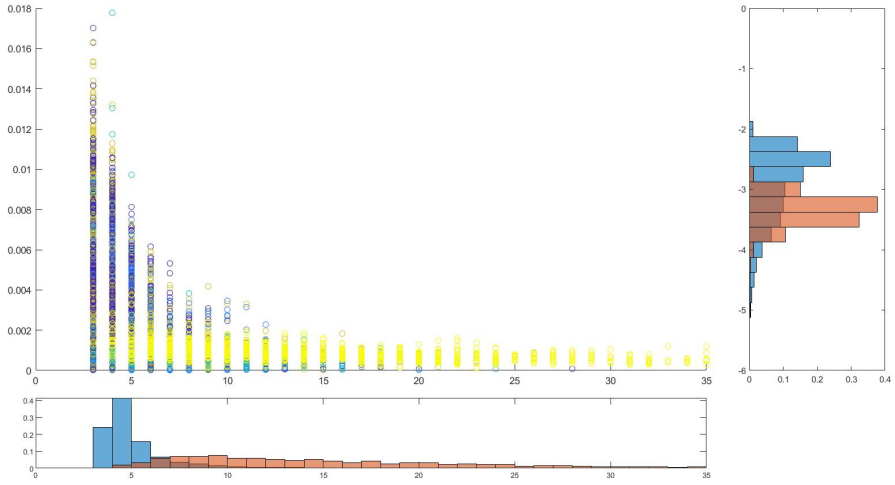

Figure 4-2: Scatter plot of stratification maximum versus FWHM for all ITP profiles in the Beaufort Gyre. Season is delineated with winter (dark blue) and summer (light blue). Remnant layer stratification and FWHM are shown in yellow. Right side panel provides a PDF of log stratification for the stratification maxima (blue) and remnant layer (red). Bottom panel shows a PDF of FWHM for the stratification maxima (blue) and remnant layer (red).

eroded, and the new remnant layer had not yet begun to form. Understanding how the stratification profile changed over the winter is crucial to understanding how the remnant layer is initialized, since the stratification profile in the late winter "sets" the initial state of the remnant layer.

Considering all profiles collected during Dec-May (Figure 4-3) the wintertime stratification maximum exhibited considerable variability. The maximum value ranged between $10^{-3} rad^2/sec^2$ and $10^{-2} rad^2/sec^2$, with depths between 20 and 50 m, and densities between 21 and 25 kg/m^3.

The magnitude of the wintertime stratification maximum was normally distributed in log space, with a mean value of approximately $2.8 \times 10^{-3} rad^2/sec^2$, and a standard deviation of $8.1 \times 10^{-3} rad^2/sec^2$. The density of the stratification maximum was also normally distributed, with a median value at 1022.77 kg/m^3. The depth of the winter stratification maximum had a wide normal distribution, showing significantly more variability than its density (Figure 4-3).

For all ITP records, the maximum stratification generally diminished during the period from December through May. To examine changes in stratification, we consider statistics

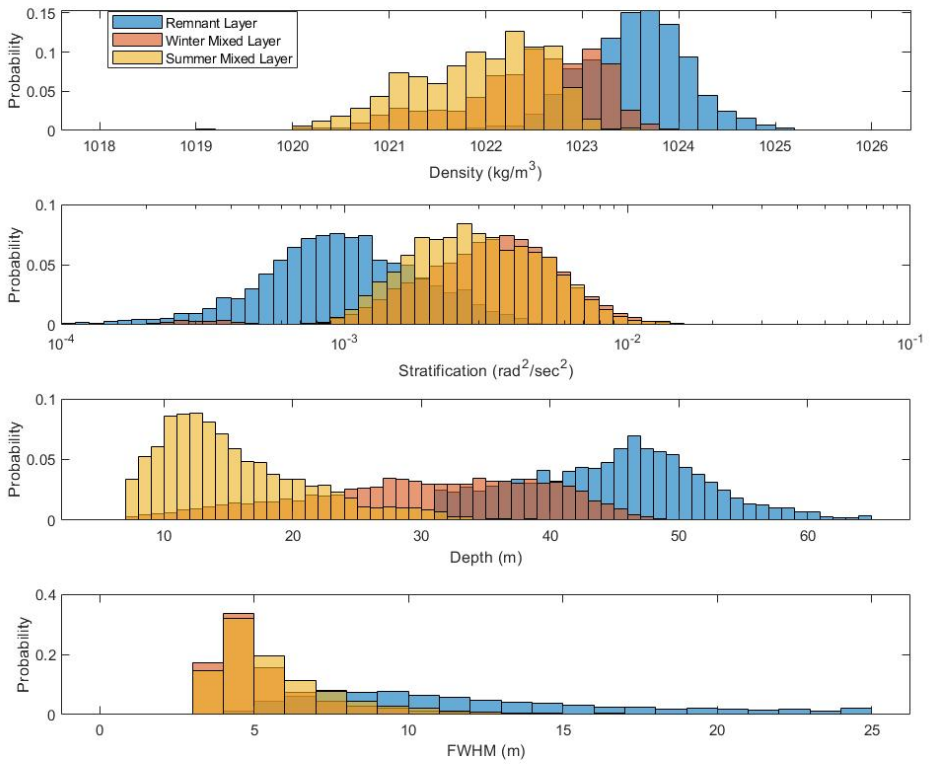

Figure 4-3: Histograms of density (top), stratification (upper middle), depth (lower middle), and FWHM (bottom) of the summer stratification maxima (yellow), winter stratification maximum (red) and remnant layer (blue).

during DJF and MAM for each ITP record. Each profile is adjusted in depth so that the stratification maxima align in depth and then profiles are averaged over DJF or MAM to produce composite stratification profiles for that month.

From DJF to MAM, the peak stratification remained relatively constant or diminished slightly over the course of the winter. Seven (33%) ITP records showed MAM maximum stratification remaining within 10% of the DJF value, and the remaining 14 ITP records (67%) showed that MAM maximum stratification decreased between 10 and 50 percent, measured relative to the DJF stratification value. Composite DJF and MAM profiles show an asymmetric stratification profile, with the stratification increasing rapidly from above to the maximum value, and then decaying away at a slower rate. Seasonality is shown in this decay as well: on average, the DJF profiles decayed to half of the maximum value in 1.70 meters above the stratification peak and in 2.94 meters below the stratification peak. This is a tighter range than the MAM months, which on average, decay to half the maximum in 2.01 meters above the stratification peak and 3.38 meters below it. Not only did the FWHM increase from DJF to MAM, but the difference between the HWHM above the stratification peak and the HWHM below the stratification peak also increased. Beneath the stratification peak, the MAM composite profiles exhibited similar variability between systems, with the stratification profiles existing in a similar range of depths and stratification values. Once beneath approximately 50 meters however, the range of stratification values was smaller (mean value of 0.8 rad^2/sec^2 vs a mean value of 0.5 rad^2/sec^2). The depth of the maximum stratification also increased by between 2 and 20 meters from DJF to MAM, depending on the ITP record (three records showed a decrease in depth). A deeper and weaker stratification peak during MAM is consistent with ice growth that increases stratification maximum layer density and depth. The larger FWHM during MAM may be caused by reduced ice formation and so reduced surface forcing that acts to compress these density surfaces. The weaker stratification during MAM suggests that halocline waters are energetically easiest to entrain during these months. The overall weakening of the stratification maximum from Dec through May shows that surface forcing is stronger than any other dynamic process such as vertical mixing that could shoal and weaken the stratification maximum. This dominant surface forcing results in significant changes in the stratification value, and more modest changes in its depth, that are consistent across ITP records. The median value of stratification in June is $3.26 \times 10^{-3} rad^2/sec^2$,which is approximately 20 percent smaller than the median value

	DJF	MAM	1Jun-15Jul	16Jul-31Aug*	SON
N2 Max ($\times 10^{-3} rad^2/sec^2$)	4.07	3.35	3.26	2.77	4.43
FWHM (meters)	4.61	5.42	5.71	6.19	4.52
$\Delta\rho$ (10 m to z_{N2max})	0.254	0.322	0.578	0.717	0.224
$\Delta\rho$ (across FWHM)	0.874	0.909	0.989	0.900	0.961

Table 4.1: Descriptive statistics for stratification profiles split by period of time, median values. *values are for the remnant stratification maximum layer

in December, $4.07 \times 10^{-3} rad^2/sec^2$.

4.1.2 June through November

Considering all profiles collected during June through November, the summertime stratification maximum had a median value of $3.5 \times 10^{-3} rad^2/sec^2$, larger than the median value during Dec-May of $3.1 \times 10^{-3} rad^2/sec^2$ (Figure 4-3). 80% of the June through November stratification values were between 1.2 and $7.0 \times 10^{-3} rad^2/sec^2$. The depth of the stratification maximum had a median value of 30 meters, with the middle 80 percent of values between 17 and 50 meters.

Conditions in June and early July prior to the formation of the summer stratification maximum layer were similar to those observed during MAM. The maximum stratification value in June and the first half of July was less than that in MAM by $1.3 \times 10^5 rad^2/sec^2$, and differing in depth by 3.1 meters (Table 4-1).

The summer stratification maximum layer shoaled abruptly during July (Figure 4-1). The summer stratification maximum layer and the stratification maximum associated with it were highly variable during Aug-Sept in depth and strength. In the time period just before the transition, the upper fifty meters of the water column became increasingly more stratified. Over a several week period, the depth of the stratification maximum shifted from roughly 50 meters to roughly 20 meters.

When the remnant stratification layer formed, its stratification diminished by a relatively significant amount, after which period it remained constant for the following months (eg Figure 4-1). After the initial decrease in magnitude, the stratification maxima of the remnant layer was approximately constant indicating that processes causing it to diffuse and to strengthen were in balance even though it was no longer directly influenced by surface forcing. The depth of the remnant layer continued to increase, roughly at the same rate as it did prior to the transition (2.3 meters/month). The remnant layer stratification in July was

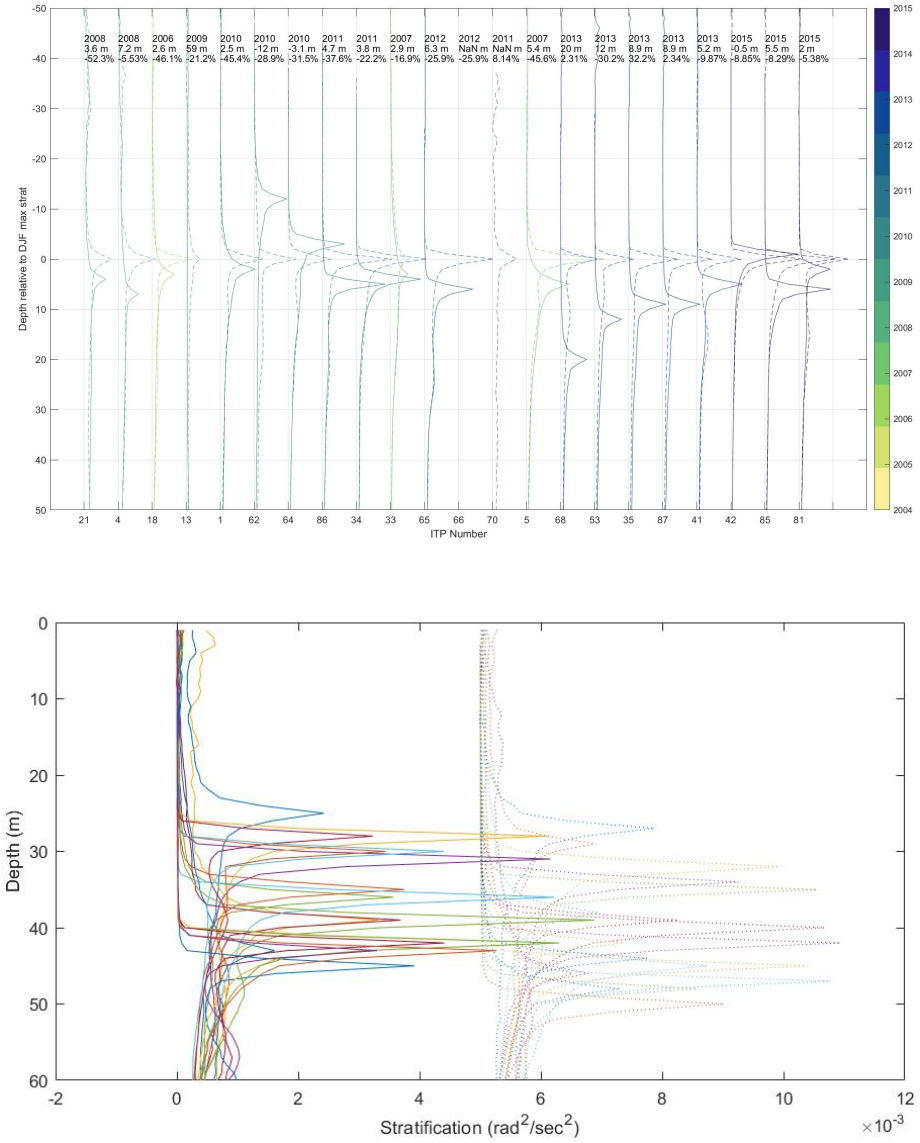

Figure 4-4: Stratification profiles from ITP records that exist in the winter months. Profiles are the average of profiles normalized to the depth of the maximum stratification (top). Profiles are sorted from lowest to highest peak stratification and offset by $3 \times 10^{-3} rad^2/sec^2$. Solid lines indicate DJF stratification. Dashed lines indicate MAM stratification. Values given are the mean change in depth from DJF to MAM and the percent change in maximum stratification from DJF to MAM. (bottom) All DJF and MAM as in the top panel but overplotted at the depth of the peak stratification. MAM profiles are offset by $5 \times 10^{-3} rad^2/s^2$

roughly two thirds of the value of the maximum stratification, at $2.1 \times 10^{-3} rad^2/sec^2$. Compared with the stratification maximum in June, the average remnant stratification maximum in July was anywhere from 1.2 to 2.2 times smaller. This variability in the extent to which the stratification layer was altered when the summer stratification maximum layer and the remnant stratification maximum layer formed, presumably results from how the transition actually occurred. The speed with which it occured or the degree to which the summer stratification maximum layer density decreased could potentially explain the variability in the remnant stratification layer.

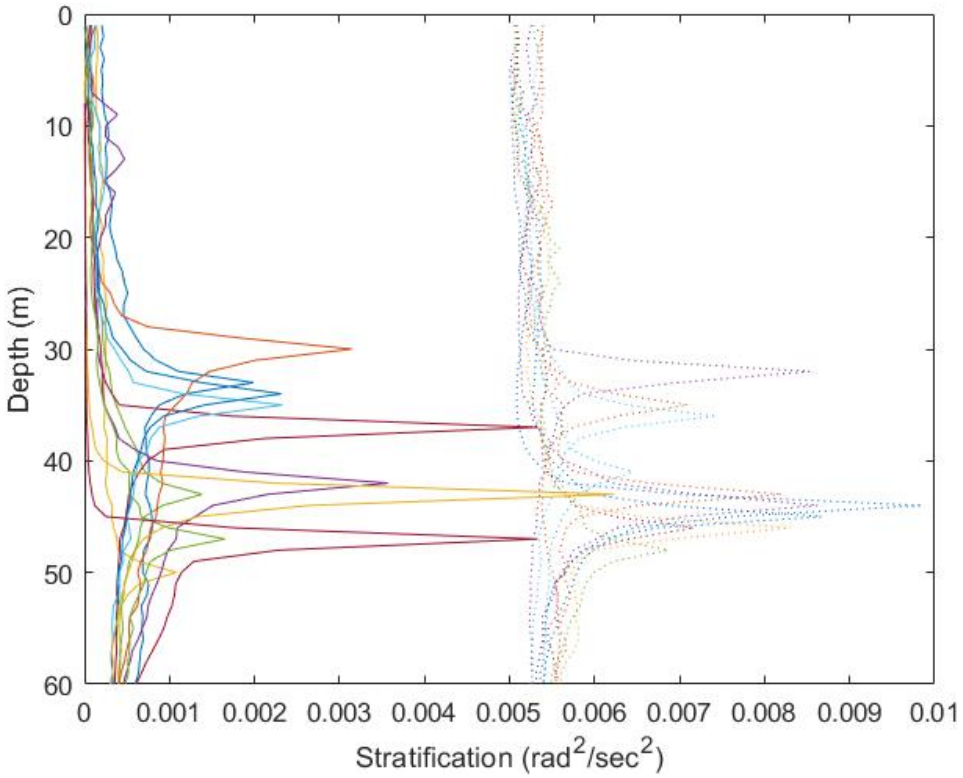

Figure 4-5: Time averaged stratification profiles in June (solid lines) and July (dashed lines, offset by $3 \times 10^{-3} rad^2/sec^2$

4.2 Transition between winter and summer

4.2.1 Formation of the remnant stratification layer

Differences between the winter stratification maximum layer and the remnant stratification maximum layer provide insights into the dominant dynamics governing the stratification

maximum layer. Several characteristics of the remnant stratification maximum layer clearly distinguish it from the winter stratification maximum layer, from which it originates. In the aggregate, the remnant stratification maximum layer is 10 meters deeper, is half as stratified, and 1.3 kg/m^3 denser than the winter maximum stratification (Figure 4-3).

PDFs for density, depth, and stratification are approximately normally distributed with the winter and remnant stratification layers different from each other at the 99 percent confidence level (Figure 4-3). The changes in density between the winter maximum stratification layer and the remnant stratification maximum layer show that the remnant layer undergoes a significant migration in density space while it deepens. The median June maximum stratification occurs at 1022.8 kg/m^3, while the median density for the remnant stratification layer occurs at 1023.9 kg/m^3. When we compare the immediately pre-transition time period (June) to the time period where the remnant layer is distinctly established (July), we continue to see several distinct differences (above the 99 percent confidence level). In the median sense, the remnant layer in July is 8 meters deeper, 1.12 kg/m^3 denser, and 1.49rad^2/sec^2 (50 percent) less stratified when compared to the stratification maximum in June (Figure 4-6).

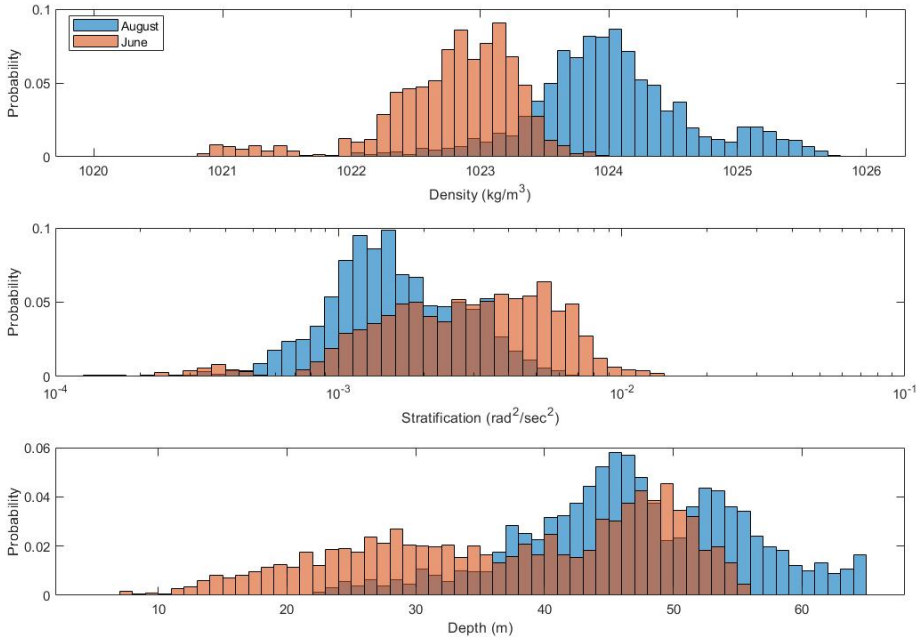

Figure 4-6: Histograms of density (top), stratification (middle), and depth (bottom) of June stratification maximum properties (blue) and August remnant layer (red).

The change in properties between the winter and remnant stratification layers takes place over the course of approximately 2-4 weeks (figure 4-9). This characteristic time scale associated with the transition was determined by constructing a composite view of the stratification before and after the transition time. By combining multiple ITP records into a single composite, variability due to smaller scale processes (Section 4.3) is reduced and a broad scale picture of the process is obtained. Composite profiles, constructed by averaging 26 ITP records together, after adjusting to the time of the transition (Figure 3) showed a period of time greater than 10 days before the transition time with approximately constant stratification of around 3-4$\times 10^{-3}$ rad^2/sec^2, and a period of time after the transition time with stratification of around 2×10^{-3} rad^2/sec^2. This was coincidental with the FWHM increasing from around 3 meters to closer to 6 meters. In this composite view, the stratification maximum began decreasing about 5-10 days before the transition occurs, which was consistent with the period of time where the stratification maximum layer was shoaling. It had fully diminished by t=0, the day when we first identified a summer stratification maximum layer (Section 3.6). The stratification roughly halved during the 5-10 days just prior to the transition time, and the FWHM increased by a factor of 1.5-2 (fig 4-9) in a 10-20 day period about the transition time. Both before and after this time period, both the stratification and FWHM remained roughly constant, indicating that the dynamical processes were in approximate equilibrium outside of the 10-20 day period surrounding the transition time.

With this time scale, we also estimated an effective vertical diffusivity, κ_v that describes how the stratification profile changed in time using a simple one dimensional model. The assumption is that prior to the transition, surface forcing that acts to sharpen the stratification approximately balances background vertical mixing that acts to weaken it. In an idealized setting, the summer stratification maximum layer forms and isolates the winter stratification maximum layer from surface forcing, leaving only the background vertical mixing to weaken the stratification in this layer. As there is a timescale of 2-4 weeks associated with the transition to a new equilibrium state, this implies that 1) vertical mixing diminishes after two weeks and was too small to diminish the remnant stratification maximum layer further, or 2) there was some presumably smaller forcing that balances whatever vertical mixing remains after this adjustment period.

We estimate diffusivity, κ_v for each ITP record that demonstrates a transition and has

ITP Number	Transition Date	Diffusivity	ITP Number	Transition Date	Diffusivity
4	6/29	0.388×10^{-6}	77	6/21	1.32×10^{-6}
5	6/18	3.80×10^{-6}	78	6/22	0.207×10^{-6}
33	6/19	0.808×10^{-6}	79	6/28	0.134×10^{-6}
41	6/27	2.38×10^{-6}	81	6/16	0.858×10^{-6}
53	6/13	0.964×10^{-6}	85	6/20	1.02×10^{-6}
62	6/6	2.45×10^{-6}	86	6/2	1.17×10^{-6}
64	6/12	0.313×10^{-6}	87	6/18	0.993×10^{-6}
65	6/8	1.70×10^{-6}	97	6/25	1.34×10^{-6}
70	6/20	0.200×10^{-6}	108	6/2	0.890×10^{-6}

Table 4.2: Transition date and effective diffusivity (m^2/sec) values for ITP records with observations of a winter to summer transition

sufficient data to generate a composite profile before and after the transition. Pre-transition and post-transition profiles are defined as an average profile (depth-normalized to the depth of maximum stratification) of the four weeks ending one week before the transition (pre-transition profile) and of the four weeks starting one week after the transition (post-transition profile). Each pre-transition profile is numerically diffused over a range of diffusivity values from 1×10^{-5} to 1×10^{-10} using the equation:

$$\frac{\partial}{\partial t} N^2(z,t) = \frac{\partial}{\partial z} \kappa \frac{\partial}{\partial z} N^2(z,t). \tag{4.1}$$

An effective diffusivity value is chosen to represent the transition period if the diffused pre-transition profile corresponding to the diffusivity value most closely matches the post-transition profile, as defined by the sum of the magnitude of difference between stratification profiles in the 9 meters centered on the stratification peak. The effective diffusivities (Table 4.2) ranged from 0.1 to 3.6 $\times 10^{-6} m^2/s$.

The effective diffusivity is very weakly negatively correlated with density in the pre-transition period ($R^2 = 0.2$) and not at all correlated with depth in the pre-transition period. It is, however, well correlated with the pre-transition stratification maximum ($R^2 = 0.51$), and the correlation is significant (P=0.02). This is likely because a stronger stratification has more ability to decay, and resulted in a larger effective diffusivity.

The dominance of vertical mixing during the transition period can also explain why the remnant stratification layer deepens. This could come about because mixing occurs that erodes the remnant layer stratification in a non-uniform way, ie, diffusion is elevated above and at the stratification maximum compared to below it, causing the stratification maximum

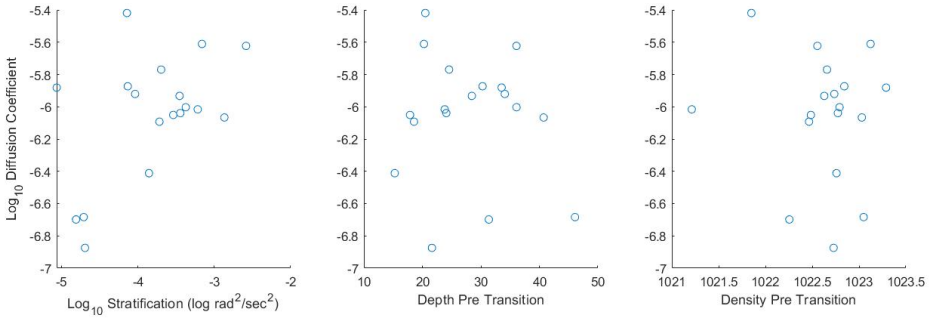

Figure 4-7: Scatter plots of effective diffusivity versus the pre-transition log stratification (left), depth of the stratification maxima (middle) and density of the stratification maxima (right) compared to the log effective diffusivity .

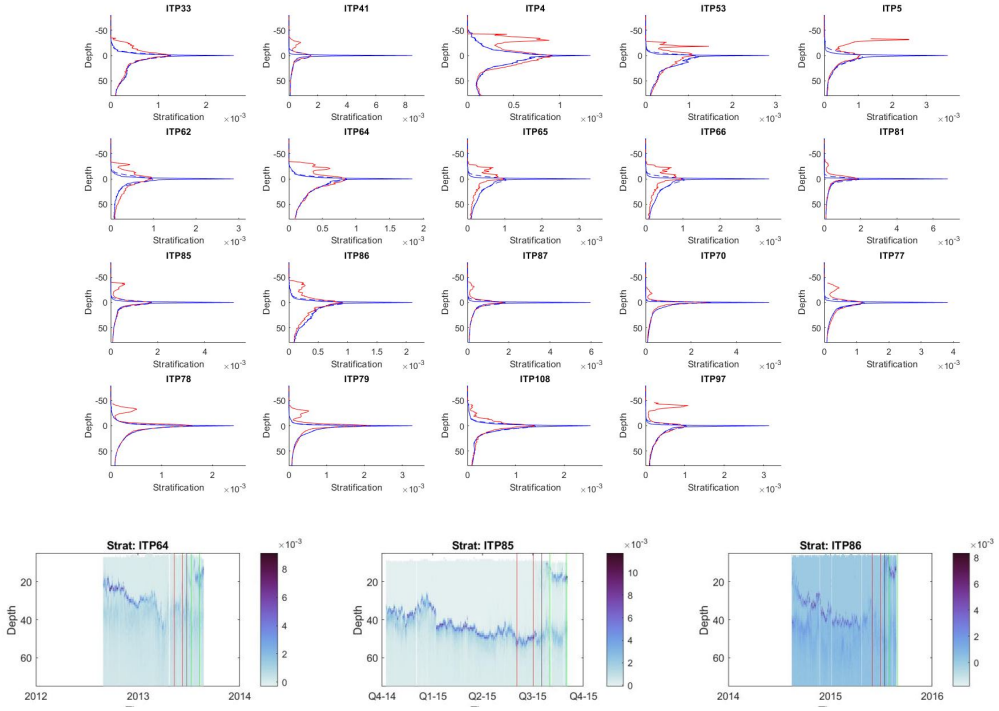

Figure 4-8: Top: Stratification profiles before transition (solid blue), after transition (solid red) and numerically diffused (dashed blue). Bottom: Log stratification profiles for selected ITP records with pre- and post-transition profile averages indicated (red) and (green).

to deepen. Alternatively, if the stratification profile is non-uniform to begin with, with a more gradual decrease in stratification below the stratification maximum, uniform diffusion would cause the depth of the maximum stratification to shift deeper as well. This non-uniform stratification profile is indeed observed (Figure 4-9), but modeled post-transition profiles do not exhibit a significant change in depth. As the remnant layer forms, the isopycnals associated with the stratification peak at the remnant layer spread out (Figure 4-8). This is consistent with the diminishing stratification observed during the transition.

Some of the differences between ITP records may be related to differences in the sea ice cover or the stratification maximum layer. Treating each record as a single datapoint, we consider relationships between the maximum stratification and characteristics of the stratification maximum layer and sea ice before and after transition times. Specifically, we examine salinity near the surface (approximately 6 meter depth), ice concentration, and ice speed (Figure 4-7). Most of these factors are only weakly correlated with the change in stratification and the time period over which the transition occurs. It is not possible to disentangle a single cause that clearly explains differences between ITP systems.

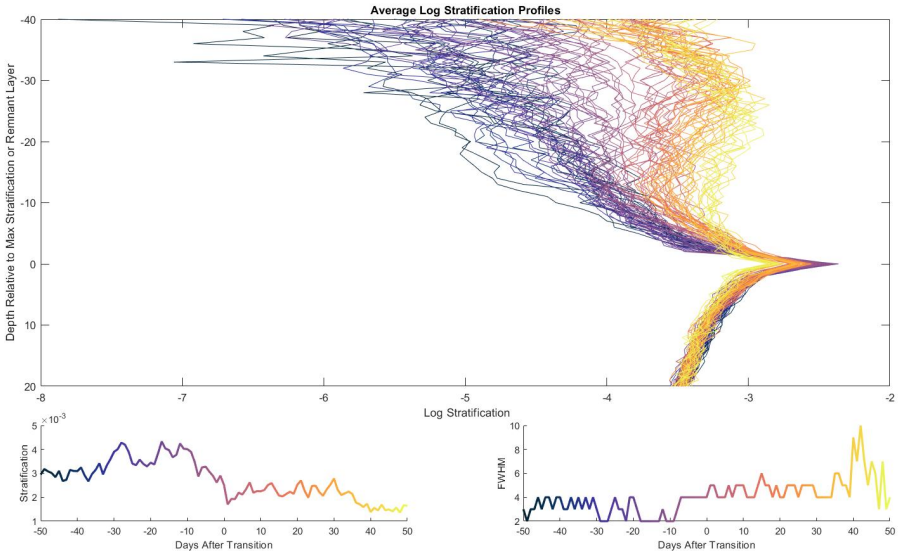

Figure 4-9: statistics constructed by averaging applicable ITP records normalized to the time of transition (summer stratification maximum layer formation) and depth of the stratification maximum or stratification maximum layer. Log Stratification with colors (dark to light)indicating time going from 50 days before the transition to 50 days after the transition. Composite statistics of (bottom left) the maximum stratification and (bottom right) the FWHM prior to and during the transition.

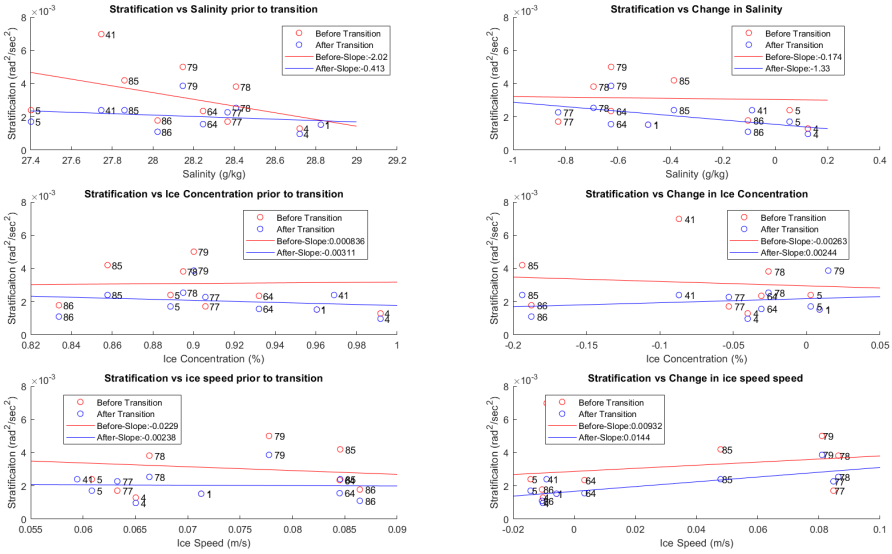

Figure 4-10: Correlations between stratification before (red dots) and after (blue dots) the transition and salinity prior to transition (top left), change in salinity across the transition (top right), ice concentration before the transition (middle left), change in ice concentration (middle right), mean ice speed prior to transition (bottom left) and change in mean ice speed (bottom right), as well as associated trend lines.

4.2.2 Oceanic Heat Content During the Transition

If, when, and to what extent upper ocean heat content is stored within or is vertically fluxed through the stratification maximum has significant implications for the ice cover. ITP records that exhibited a transition were considered, and heat content was considered both before and after the transition time. In the pre-transition time, heat content was considered in two parts: surface to the base of the stratification maximum layer, and the stratification maximum layer base to the 1025 isopycnal, which is roughly the location of the Pacific Summer Water. This isopycnal occurs around 100 meters depth, and is stable year round. In the post-transition time, heat content was considered from the surface to the base of the stratification maximum layer, the base of the stratification maximum layer to the top of the remnant layer (defined as the upper portion of the FWHM for the remnant layer), the remnant layer (upper FWHM to lower FWHM) and from the bottom of the remant layer to the Pacific Summer Water (again defined as the 1025 kg/m^3 isopycnal). These regions were chosen because they represent oceanic heat content of varying levels of accessibility. For each ITP record, the total heat content of the upper portion of the water

column (surface to the 1025 kg/m^3 isopycnal is relatively constant throughout the time period being considered (namely, two months about the transition time), with perhaps some slight seasonal trends and small scale variability. The variability between the ITP records in terms of total heat content is explained by the varying depth of the 1025 isopycnal and the varying temperature within the PSW layer. Seasonally, there is some potential for heat to transfer into the remnant stratification maximum layer from below, but for the most part, there were no significant changes in heat content at the transition time:o the remnant heat content builds up over longer timescales after the transition time. However, heat content was observed within both the upper and lower portion of the remnant stratification maximum.

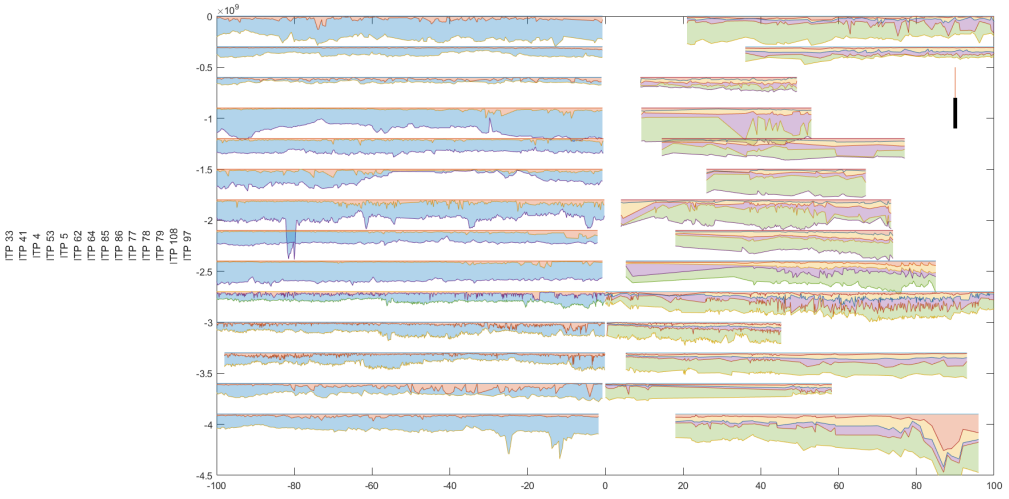

Figure 4-11: Heat content for ITPs about the winter - summer transition. Black bar indicates $3 \times 10^8 J/m^2$. The heat content is shown for the mixed layer base (red), mixed layer base to PSW isopycnal (blue), mixed layer base to remnant layer upper FWHM (yellow), within the remnant layer (purple), and the lower remnant layer FWHM to PSW isopycnal.

We can examine this in slightly more detail by considering how isopycnals behave with respect to the heat content during the transition (Figure 4-12). Isopycnal spreading, with the associated heat content, shows a mechanism for how heat from the lower portion of the ocean enters into the remnant layer. As isopycnals spread, they bring with them some of the heat in the lower layers. The end result is that a non trivial amount of heat is now captured on top of the remnant layer stratification peak, and from there, can be more easily diffused into the relatively weakly stratified region that is the remnant layer.

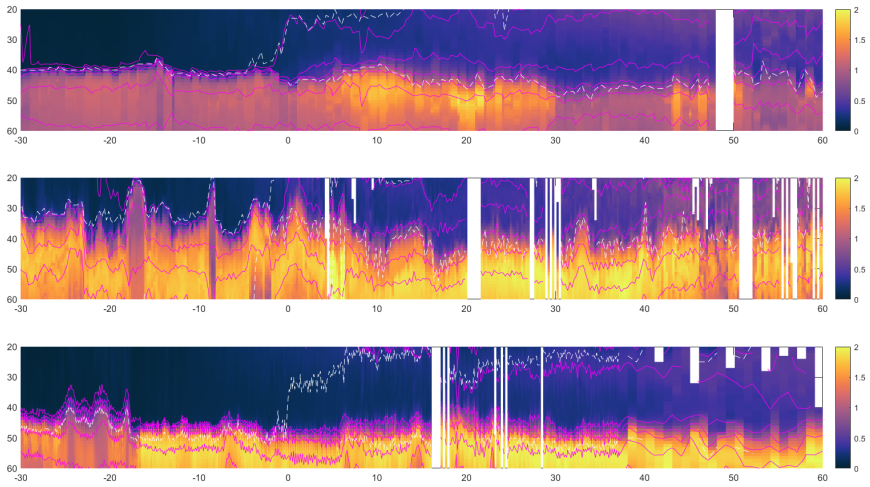

Figure 4-12: Temperature above freezing displayed as a function of depth and days away from the transition for ITPs 41 (top) 64 (middle) and 78 (bottom). Isopycnals are shown in pink. Stratification maximum and remnant layer base are shown in dashed white.

4.3 Interannual Variability

The broad seasonal changes are similar in pattern across the ITP records examined, though there are variations the physical quantities (like stratification, density, or temperature) take and the timings at which these seasonal changes occur. The profile to profile differences in stratification are non-trivial. Here, we examine interannual variability by considering two year groups, 2005-2010 and 2011-2018.

In both year groups identified, as well as the mean over all years, the stratification maximum occurs in the Sep-Nov time span, and the stratification minimum occurs in the Jun-Aug time span.

Interannual changes were observed in the maximum stratification value for all months. The stratification maximum values were larger during 2011-2018 compared with 2005-2010 by as much as 30 %. However, significant overlap did exist in the two year groups.

The seasonal cycle did not exhibit interannual changes. In both year groups, the stratification maximum occurred in the Sept-Nov time span, and the stratification minimum occured in the Jan-August time span.

While this large scale interannual trend exists, we note that large scale variability exists within these periods. Even in similar time periods, there is large variability in each month

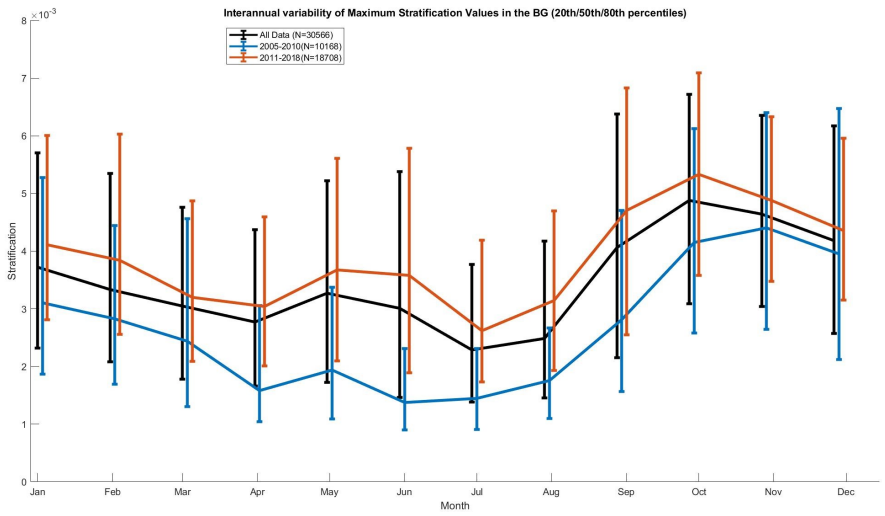

Figure 4-13: Median, 20th, and 80th percentiles of the maximum value of stratification in each month for two time periods: 2005-2010 (blue) and 2011-2018 (red) and overall (black).

examined (figure 4-13) due in part to the small scale variability that exists for different ITPs. It is important to note that each monthly statistic shown in encompasses a significant range of values. The aggregate statistic is not the most representative of the each individual record, since routinely the median of an individual record is outside the aggregate statistic 20th or 80th percentiles (fig (4-16)). However, the inter-annual differences are well represented in these individual statistics.

The remnant layer stratification maxima exhibits interannual variability as well, in terms of magnitude. Like with the stratification maxima, the remnant layer shows slightly higher stratification values, possibly as a result of the remnant layer being formed from a layer of higher stratification. There also appears to be a change in the seasonal cycle, but this is likely caused from a scarcity of data from the remnant layer in the late winter, and thus, no strong results can be drawn.

Likewise, the behavior of the FWHM for the stratification maxima and the remnant layer are similar over the time periods considered. A lack of data in the earlier period makes drawing strong conclusions difficult, but it is apparent that generally speaking, the FWHM stays at the same value between the two year periods considered.

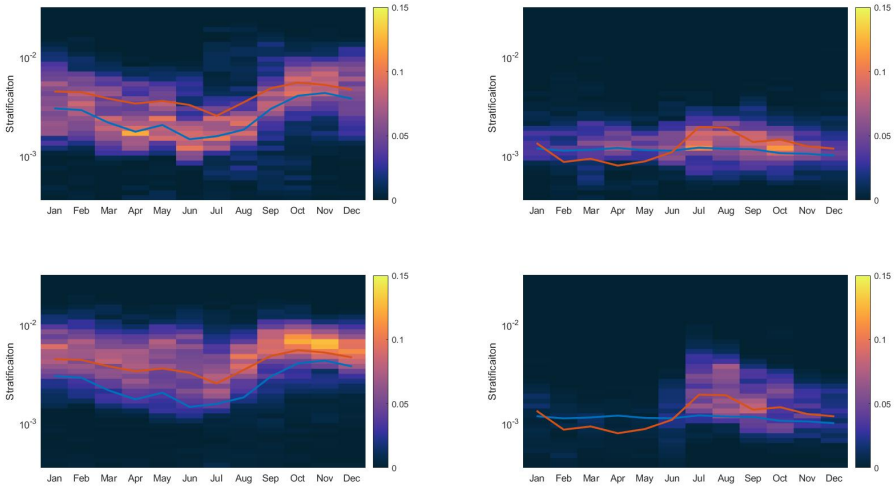

Figure 4-14: Seasonal and inter annual variability in maximum stratification (left) and remnant layer stratification (right) described by relative probability of appearance. Two timeperiods are considered: 2005-2010 (top), and 2011-2018 (bottom). Lines indicate medians for the earlier time period (blue) and the later time period (red).

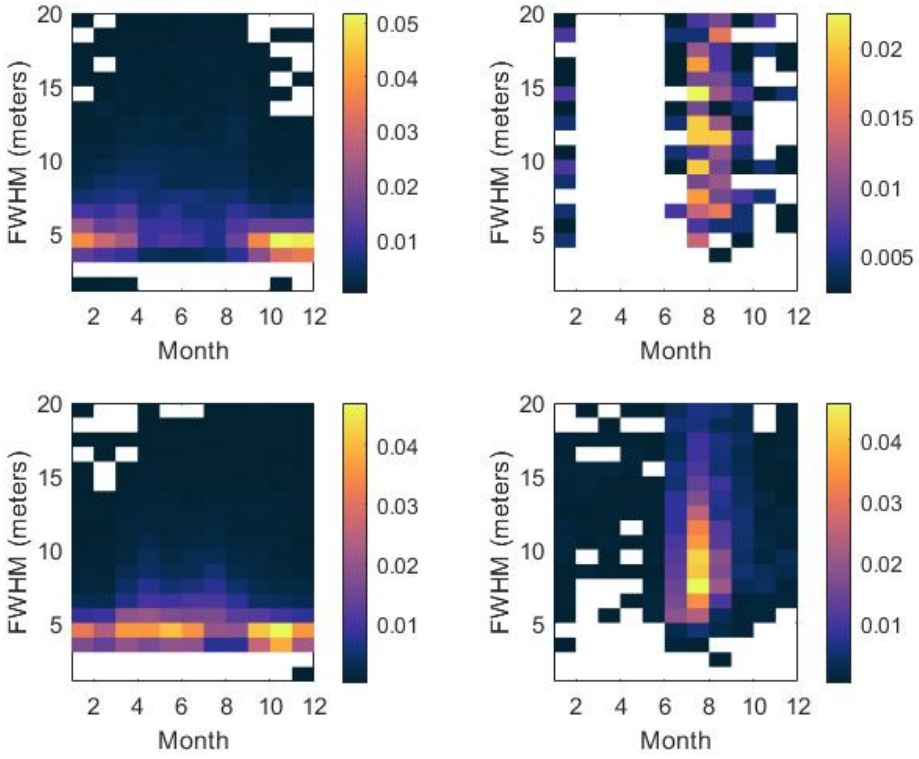

Figure 4-15: As in Figure (4-14), but with FWHM

.

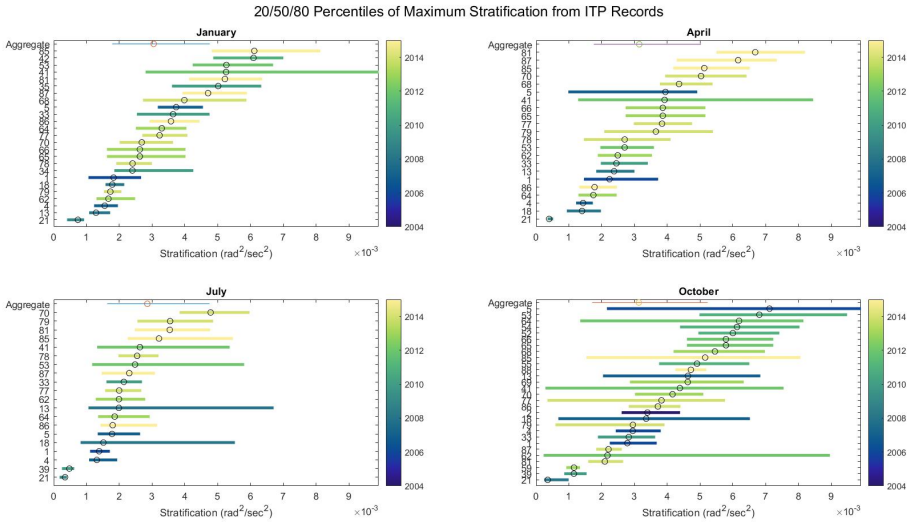

Figure 4-16: The 20th, 50th, and 80th percentile values of maximum stratification for Jan (top left), April (top right), July (bottom left), and October (bottom right) for individual ITPs color coded by year. Each bar indicates a separate ITP record

4.4 Geographic Variability

The geographic variability of the maximum stratification and the remnant layer stratification had no clear spatial pattern, at least at the basin scale level from the available observations (4-17). This suggests that the large scale causes of stratification changes were not related to location. However, it must be noted that the geographic coverage of various ITP records was relatively sparse. The records examined cover a period from 2004 to 2018, and when gridded in the Beaufort Gyre into boxes roughly 100km on a side, only a few boxes saw coverage over long periods of time (eg, ten years or more). Looking at a finer time scale, no season (DJF/MAM/JJA/SON) saw coverage in a grid box more than seven years, with fall being the most represented and spring the least represented. Thus, while the data suggests no clear spatial pattern to the stratification maxima, this is based on sparse data, and future studies may reach a different conclusion. In the aggregate, interannual variability is smaller than the seasonal variability, and geographic variability, while it does not display a consistent spatial pattern, is of similar magnitude to variability observed between profiles due to small-scale features

While no clear geographic variability is evident in the aggregate, individual sections do exhibit such variations. Consider the case of ITP 62, which transited up on the shelf for a

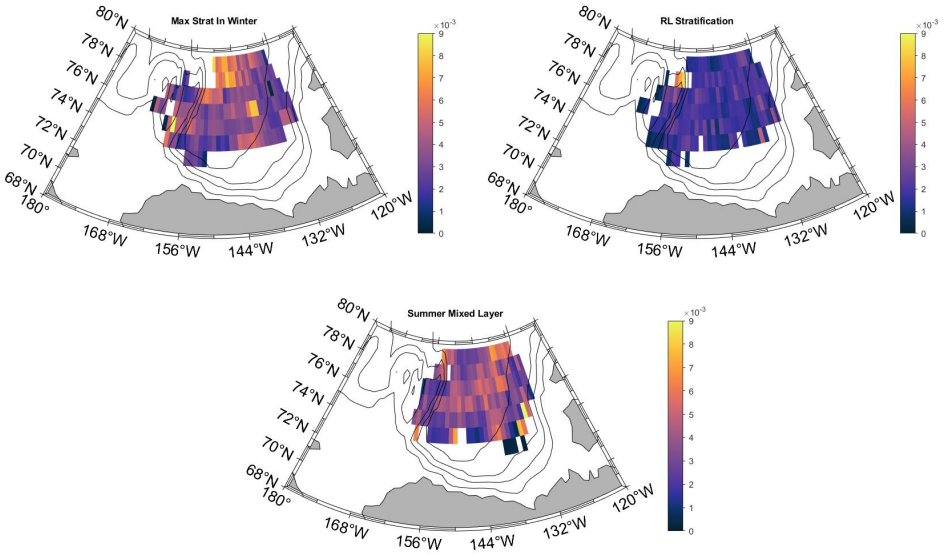

Figure 4-17: Top: The median value of the maximum stratification of all profiles occurring in a 3 degree longitude by 1 degree latitude grid square in winter (December through May). Top Right: The median value of stratification at the remnant layer for all profiles occurring in a 3 degree by 1 degree grid square. Bottom: The median value of the maximum stratification of all profiles occuring in a 3 degree longitude by 1 degree latitude grid square in summer (June through November).

period of several weeks in late spring of 2013, observing different watermasses during this time. In this instance, we see highly variable isopycnal depth changes and consequently large amounts of variability in the stratification maximum. We also see that the separation between isopycnals is much more apparent than it was in the interior of the Beaufort Gyre in June when the ITP is located further north and in deeper waters.. The stratification maximum also changed as eddies transition into the Beaufort Gyre on the northern edge. This movement into the gyre is also associated with changes in temperature and salinity (not directly shown).

4.5 Small Scale Variability

ITP records show variability on smaller spatial and temporal scales, on the order of 1-10 km and 1-10 days. Variability in properties of the stratification maximum layer can be associated with eddies and internal waves (in addition to persistent fronts discussed in Section 4.4). A systematic investigation of the eddies or internal waves is beyond the scope of the current

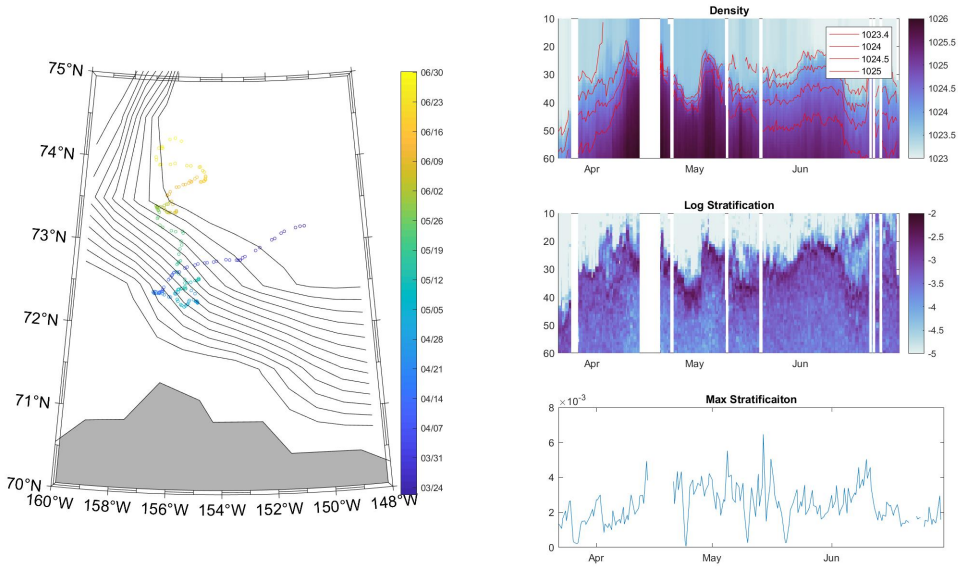

Figure 4-18: LEFT: Map of ITP 62 profile locations in early spring of 2013. Bathymetry shown in 100m contours. RIGHT: Timeseries of density with specific contours in red , stratification, and maximum stratification.

work, and has been undertaken elsewhere for the Beaufort Gyre region (Zhao et al., Dosser et al.). Here, we aim to understand the extent to which small-scale processes modify the stratification maximum layer and could either hinder or ease the transfer of heat from the halocline to the stratification maximum layer. Consider first the relationship between timescale and the magnitude of variability of the stratification maximum layer (Figure 4-19). As we move from larger time scales to smaller time scales, we see magnitude of variation that the stratification profile can exhibit at each time scale. Over the course of a year, the stratification maximum layer depth changes by about 50 meters, due to the seasonal cycle. For an example time period of roughly two weeks, the depth varies by about 10 meters. Thus, we can say that the magnitude of variability in depth is only loosely correlated with the time scale. Similarly, the maximum stratification value exhibits significant variability on a two-week timescale.

4.5.1 Eddies

The impact of eddies on the stratification profile is illustrated using data from ITPs 35, 78, and 79. These records sample at relatively high frequency (once every three or four hours).

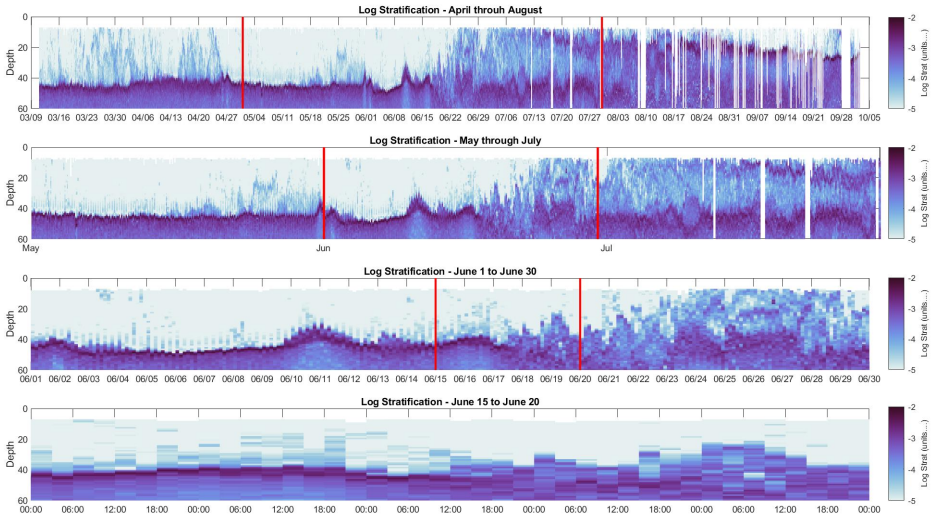

Figure 4-19: Timeseries of log stratification for ITP 64 shown for depths of 10-60m during spring through summer (top panel), summer (second panel), June (third panel), and a two week period in June (bottom panel). Red lines indicate time period covered by the lower panel.

ITPs 78, and 79 records are overlaping in time (during 2014), while ITP 35 occurred earlier (2009-2010), and in a similar region in the Beaufort Gyre. Within the Beaufort Gyre, the Rossby deformation radius is approximately 13 km (Zhao et al.), and the eddies are comparably sized (e.g., Figure 4-20). ITPs generally do not travel in straight lines, and often the path through the eddy does not include the center, so there is variability in the amount of time an ITP spends in any individual eddy. Several features characterize an eddy on the ITP record. Isopycnals shift in depth, in some cases by as much as 10 meters. Stratification is most strongly influenced within the eddy, where it decreases as a results of isopycnals being stretched apart. The most significant impact, as seen in Figure 4-20, is that the depth of the stratification maximum changes by meters, but there is no indication that the magnitude of the stratification maximum changes significantly.

Consider the eddy that occurs on June 21st, 2014 for ITP 78. This eddy caused the isopycnals from approximately 1023.4 through 1025 to shoal. At the same time, the magnitude of maximum stratification showed no significant changes within versus outside of the eddy. Contrast this with the eddy that occurs around June 24th, 2014 for ITP 78. This shows the 1023.4 and 1024 isopycnals decreasing in depth by approximately 5 meters, the 1024.5 isopycnal remaining at roughly the same depth, with some minor fluctuations, and

the 1025 isopycnal increasing in depth by up to 18 meters. The maximum stratification increased within the eddy in this case.

Overall, examples exist of eddies with either increased, similar, or decreased stratification. The depth at which the eddy occurs likely plays a role in shaping the impact on the stratification maximum layer. Eddies that are deep have either limited impact on the maximum stratification, because if isopycnals near the stratification maximum layer are moved, the movement occurs in a uniform manner, or they act to increase stratification as the isopycnals are compressed near the stratification maximum layer (which is where the maximum stratification occurs). Eddies that are shallower seem to have a tendency to diminish the maximum stratification, since the isopycnals are spreading near where the maximum stratification occurs. While the total number of eddies is relatively small.

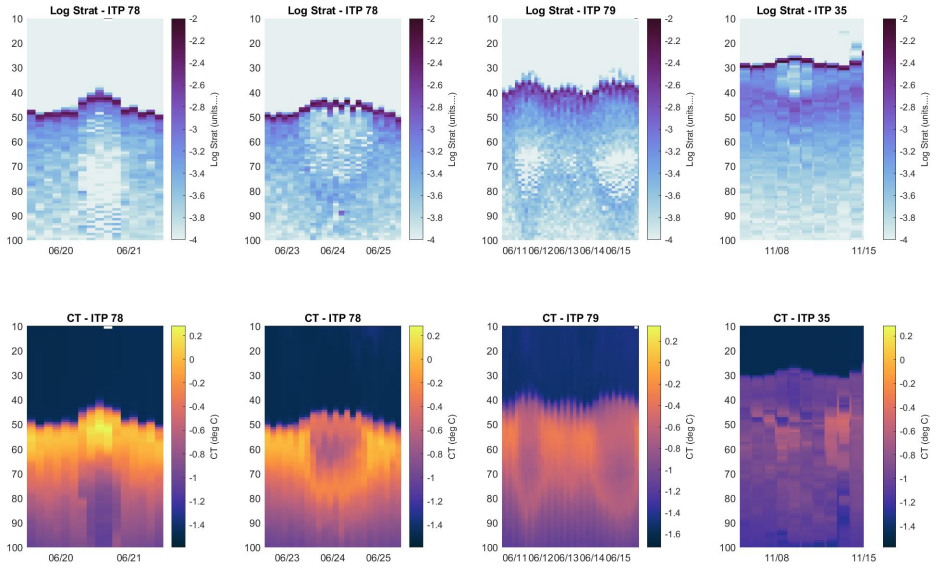

Figure 4-20: Time series of log stratification (top) and conservative temperature (bottom) for four eddies from ITPs 78, 79, and 35.

4.5.2 Internal Waves

Internal waves in the Arctic are primarily near inertial, and oscillate at a frequency near 12 hours. We would expect this oscillation to change the depth of the stratification maximum, but maintain the magnitude roughly intact. Some magnitude changes could be expected by the stretching and compression of the density surfaces over the internal wave period. To

illustrate this point, we examine a two week period in June of 2014 from ITP 77 (Figure 4-21). Here, we see the oscillation in depth space of the isopycnals, while the magnitude of the stratification remains relatively constant .

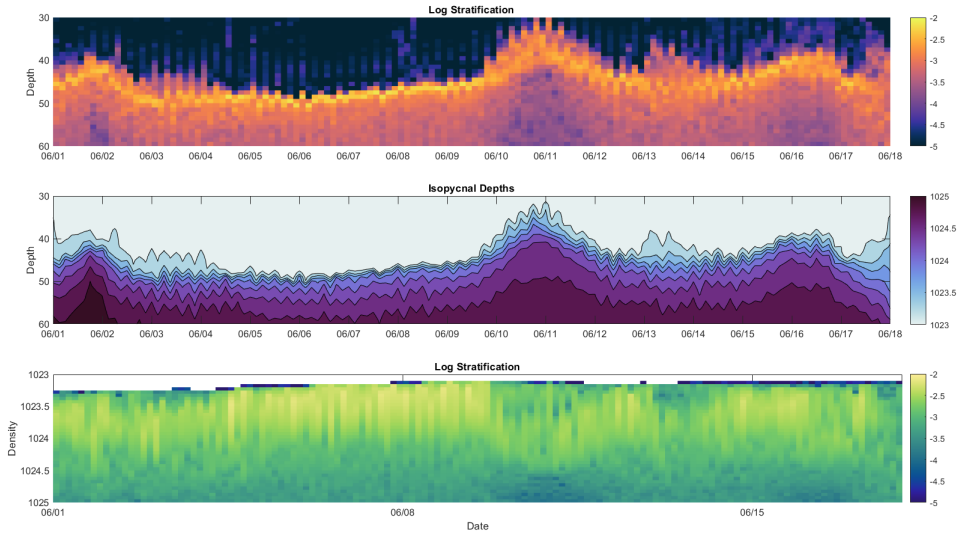

Figure 4-21: Time series of log stratification (top), density (middle) and log stratification in density space (bottom) for ITP 77, a high resolution ITP in June of 2014.

Chapter 5

Discussion and Conclusions

Properties of the stratification maximum layer exhibited a wide range of values. The thickness of the stratification maximum layer was most constant, a median values of 5.08 m, and density of 1022.1 kg/m^3. The median value of the stratification maximum was $3.39 \times 10^{-3} rad^2/sec^2$, with 10 and 90 percentiles at $1.33 \times 10^{-3} rad^2/sec^2$ and $6.71 \times 10^{-3} rad^2/sec^2$. Over the entire record, the depth and density of the stratification maximum varied from 7 to 50 m and 1020 to 1025 kg/m^3. Basin scale geographic variability was not evident in these properties, so variability results primarily from small-scale, seasonal, and interannual effects.

A strong seasonal cycle in surface forcing governs the seasonal evolution of the stratification maximum layer. The stratification maximum reached its highest value in October, with a median value of $4.8 \times 10^{-3} rad^2/sec^2$, when it had a mean depth of 20 m. From October through June, the stratification decreased in value to $2.3 \times 10^{-3} rad^2/sec^2$, and increased in depth to 41 meters. A steady state was not observed at any time during October – June, suggesting that surface forcing and interior vertical mixing never reached an equilibrium. The summer mixed layer shoaled during late June, with transition times that ranged between 10 and 14 days. The summer stratification maximum layer had similar maximum values to winter months that ranged between $1 - 10 \times 10^{-3} rad^2/sec^2$. The remnant stratification maximum layer formed in June, was not mixed away during the summer months, and was re-entrained into the following winter's stratification maximum layer. The remnant stratification layer was characteristically wider, weaker, and deeper than the mixed layer, with stratification maxima that were slightly deeper (47 vs 41 meters), significantly denser

(1024 vs 1023 kg/m^3), FWHM of 12 m (compared to the stratification layer FWHM of 4 m), and stratification values centering around $1 \times 10^{-3} rad^2/sec^2$. These new properties were quickly established over an approximately 10 day period around the time that the summer mixed layer shoaled. This abrupt change followed by an approximately steady state suggests that a balance between restratification and diffusion dynamics in the interior of the upper portion of the water column is achieved shortly after the summer mixed layer shoals.

Interannual variability was examined by considering two timeperiods: 2005-2010 and 2011-2018. The basic seasonal cycle was the same over each time period examined: a slow deepening and weakening of a stratification maxima from October through June, followed by a period where the stratification rapidly becomes shallow in late June and strengthens through October. There was no significant difference in depth between the two time periods examined, but the mean values of stratification were higher for the later time period by 1 to $2 \times 10^{-3} rad^2/sec^2$. The two timeperiods were not completely distinct, and exhibited some overlap in properties. The remnant layer showed slight changes between the two time periods as well, with the later years having had a slightly more stratified remnant layer stratification peak than the earlier years. The time period over which the transition occurred showed no significant interannual variability, happening in the same period of time regardless of year.

We have not identified a specific cause of the interannual variability. There are likely many factors beyond the scope of this study that could cause it, including melt rates, surface temperatures, or changes in mixed layer density. In the interannual sense, there are not any explicit correlations between the depth or magnitude of stratification to larger scale processes like Beaufort Gyre freshwater content or the Arctic Oscillation Index or sea level pressure (not shown). However, it is clear that this region and processes influencing the mixed layer and halocline stratification are undergoing changes. The process level changes are likely correlated to the basin scale changes, though the exact mechanism is not clear.

The ambiguity in the connection between the basin process and the properties of the stratification maximum layer is due in part to the sparsity of data coverage. ITP coverage is variable, both temporally and spatially. Lacking repeated coverage in a specific region prevents strict comparison between characteristics associated with the water column and characteristics of the basin. Because of this, we had to group several years of observations together to investigate interannual variability. This also leads to some uncertainty in the ability to draw large scale conclusions about the timing of the transition from winter to

summer, due to only 16 records that observed this transition.

An effective diffusivity on the order of $1 \times 10^{-6} m^2/s$ was estimated based on the initial evolution of the remnant stratification maximum layer. There is significant uncertainty in the specific value in part due to uncertainty in the timescale associated with this transition and diffusivity estimate. Estimates of vertical diffusivity applicable to the base of the mixed layer are typically difficult to directly observe and we note here that it is similar to or smaller than parameterized vertical diffusivities of the interior Arctic Ocean (e.g., (et al, 2013). A vertical diffusivity of this value applied to the remnant stratification maximum layer from July through October would have minor impacts on the heat and stratification of this layer, consistent with the nearly steady state of this layer observed afters its initial adjustment. It is also possible that vertical mixing after this initial adjustment period is weaker than $10^{-6} m^2/s$.

Heat within the stratification maximum layer exhibited significant variability. As the density of the stratification maximum layer increased during winter, increased heat content was observed within the stratification maximum layer. It is not clear from this analysis alone the extent to which some of this heat is gradually or sporadically transferred to the mixed layer above. There is certainly a potential for heat transfer to the mixed layer in spring, and to the remnant mixed layer in summer. As the remnant stratification maximum layer initially moves to a denser isopycnal from where it was previously, Pacific Summer Water heat has an increased ability to mix onto lighter density surfaces. As Pacific Summer Water warms and shoals interannually, the specific dynamics of the stratification maximum layer will become increasingly important to understanding heat transfer into the mixed layer or remnant mixed layer.

The stratification in the mixed layer and the remnant layer serves to insulate the surface of the ocean from the warmer, deeper, Pacific Summer Water. Consequently, the evolution of the stratification profile plays a large role in how easily this heat content beneath the mixed and remnant mixed layers can reach the surface, where it could impact the surface ice cover. Historically, the PSW is becoming more accessible, especially in the early spring. This migration of accessibility, coupled with the shifting of the transition time period due to earlier ice melt could play an oversized role in bringing PSW heat to the surface.

Many models, especially those that describe global circulation, have vertical resolutions that are too large to accurately reflect the stratification dynamics in the upper sixty meters

of the water column in the Beaufort Gyre. This need to parameterize the remnant layer and the heat transfer through it could have significant impacts on how models describe the evolution of the heat content of the upper ocean, and subsequent ice formation and melt. Further exploration is necessary for a more complete understanding of how the uppermost layers of heat and stratification will continue to evolve in the future. Process models may be a useful tool to investigate some of the questions raised here.

While ice growth and melt will remain features of the Beaufort Gyre for many years to come, it is likely that climate change will alter the amount of ice formation, and the timing at which it occurs. The timing of the transition between the mixed layer and the remnant mixed layer may change, and so there does exist potential for the transition to happen earlier in the year in particular. How these changes could affect the remnant stratification maximum layer, and then influence the stratification maximum layer the following winter remain unexplored.

Bibliography

K. E. Brainerd and M. C. Gregg. Diurnal restratification and turbulence in the oceanic surface mixed layer. *Journal of Geophysical Research Oceans*, 98(C12):22645–22656, 1993.

Judith A. Curry, Julie L. Schramm, and Elizabeth E. Ebert. Sea ice-albedo climate feedback mechanism. *Journal of Climate*, 8(2):240 – 247, 1995.

Sarah Dewey, James Morison, Ronald Kwok, Suzanne Dickinson, David Morison, and Roger Andersen. Arctic ice-ocean coupling and gyre equilibration observed with remote sensing. *Geophysical Research Letters*, 45(3):1499–1508, 2018.

Kathleen Dohan and Russ E. Davis. Mixing in the transition layer during two storm events. *Journal of Physical Oceanography*, 41(1):42 – 66, 2011.

Guthrie et al. Revisiting internal waves and mixing in the arctic ocean. *Journal of Geophysical Research*, 2013.

Albert Buixadé Farré, Scott R. Stephenson, Linling Chen, Michael Czub, Ying Dai, Denis Demchev, Yaroslav Efimov, Piotr Graczyk, Henrik Grythe, Kathrin Keil, Niku Kivekäs, Naresh Kumar, Nengye Liu, Igor Matelenok, Mari Myksvoll, Derek O'Leary, Julia Olsen, Sachin Pavithran.A.P., Edward Petersen, Andreas Raspotnik, Ivan Ryzhov, Jan Solski, Lingling Suo, Caroline Troein, Vilena Valeeva, Jaap van Rijckevorsel, and Jonathan Wighting. Commercial arctic shipping through the northeast passage: routes, resources, governance, technology, and infrastructure. *Polar Geography*, 37(4):298–324, 2014.

K. E. Frey, J. C. Comiso, L. W. Cooper, J. M. Grebmeier, and L. V. Stock. Arctic ocean primary productivity: The response of marine algae to climate warming and sea ice decline. *Arctic Report Card 2020*, 2020.

T. M. Shaun Johnston and Daniel L. Rudnick. Observations of the transition layer. *Journal of Physical Oceanography*, 39(3):780 – 797, 2009.

R. Krishfield, J. Toole, A. Proshutinsky, and M-L. Timmermans. Automated ice-tethered profilers for seawater observations under pack ice in all seasons. *Journal of Atmospheric and Oceanic Technology*, 25(11):2091 – 2105, 2008a.

R. Krishfield, J. Toole, A. Proshutinsky, and M-L. Timmermans. Automated ice-tethered profilers for seawater observations under pack ice in all seasons. *Journal of Atmospheric and Oceanic Technology*, 25(11):2091 – 2105, 2008b.

R. A. Krishfield, A. Proshutinsky, K. Tateyama, W. J. Williams, E. C. Carmack, F. A. McLaughlin, and M.-L. Timmermans. Deterioration of perennial sea ice in the beaufort gyre from 2003 to 2012 and its impact on the oceanic freshwater cycle. *Journal of Geophysical Research: Oceans*, 119(2):1271–1305, 2014.

R Kwok. Arctic sea ice thickness, volume, and multiyear ice coverage: losses and coupled variability (1958–2018). *Environmental Research Letters*, 13(10):105005, oct 2018.

Guancheng Li, Lijing Cheng, Jiang Zhu, Kevin E. Trenberth, Michael E. Mann, and John P. Abraham. Increasing ocean stratification over the past half-century. *Nature Climate Change*, 10(12):1116–1123, 2020.

Trevor J. McDougall. The relative roles of diapycnal and isopycnal mixing on subsurface water mass conversion. *Journal of Physical Oceanography*, 14(10):1577 – 1589, 1984.

Gianluca Meneghello, John Marshall, Jean-Michel Campin, Edward Doddridge, and Mary-Louise Timmermans. The ice-ocean governor: Ice-ocean stress feedback limits beaufort gyre spin-up. *Geophysical Research Letters*, 45(20):11,293–11,299, 2018.

A. Proshutinsky, R. Krishfield, J. M. Toole, M.-L. Timmermans, W. Williams, S. Zimmermann, M. Yamamoto-Kawai, T. W. K. Armitage, D. Dukhovskoy, E. Golubeva, G. E. Manucharyan, G. Platov, E. Watanabe, T. Kikuchi, S. Nishino, M. Itoh, S.-H. Kang, K.-H. Cho, K. Tateyama, and J. Zhao. Analysis of the beaufort gyre freshwater content in 2003–2018. *Journal of Geophysical Research: Oceans*, 124(12):9658–9689, 2019.

Koji Shimada, Takashi Kamoshida, Motoyo Itoh, Shigeto Nishino, Eddy Carmack, Fiona McLaughlin, Sarah Zimmermann, and Andrey Proshutinsky. Pacific ocean inflow: Influence on catastrophic reduction of sea ice cover in the arctic ocean. *Geophysical Research Letters*, 33(8), 2006.

F. Sévellec, A. Fedorov, and W. Liu. Arctic sea-ice decline weakens the atlantic meridional overturning circulation. *Nature Clim Change*, pages 604–610, 2017.

Richard E. Thomson and Isaac V. Fine. Estimating mixed layer depth from oceanic profile data. *Journal of Atmospheric and Oceanic Technology*, 20(2):319 – 329, 2003.

M.-L. Timmermans, A. Proshutinsky, E. Golubeva, J. M. Jackson, R. Krishfield, M. McCall, G. Platov, J. Toole, W. Williams, T. Kikuchi, and S. Nishino. Mechanisms of pacific summer water variability in the arctic's central canada basin. *Journal of Geophysical Research Oceans*, 119(11):7523–7548, 2014.

John M. Toole, Richard A. Krishfield, Mary-Louise Timmermans, and Andrey Proshutinsky. The ice-tethered profiler: Argo of the arctic. *Oceanography*, 24(3):126–135, 2011. ISSN 10428275, 2377617X.

Ryohei Yamaguchi and Toshio Suga. Trend and variability in global upper-ocean stratification since the 1960s. *Journal of Geophysical Research: Oceans*, 124(12):8933–8948, 2019.